

1 **Multi-year monitoring of atmospheric TGM at a remote high-**
2 **altitude site (Nam Co, 4730 m a.s.l.) in the inland Tibetan Plateau**

3 Xiufeng Yin ^{1,2,3,4}, Shichang Kang ^{1,5}, Benjamin de Foy ⁴, Yaoming Ma ^{2,5}, Yindong Tong ⁶, Wei Zhang
4 ⁷, Xuejun Wang ⁸, Guoshuai Zhang ², Qianggong Zhang ^{2,5}

5 ¹State Key Laboratory of Cryospheric Science, Northwest Institute of Eco-Environment and Resources, Chinese Academy of
6 Science, Lanzhou, 730000, China

7 ²Key Laboratory of Tibetan Environment Changes and Land Surface Processes, Institute of Tibetan Plateau Research, Chinese
8 Academy of Sciences, Beijing, 100101, China

9 ³University of Chinese Academy of Sciences, Beijing, 100039, China

10 ⁴Department of Earth and Atmospheric Sciences, Saint Louis University, St. Louis, MO, 63108, USA

11 ⁵CAS Center for Excellence in Tibetan Plateau Earth Sciences, Beijing, 100101, China

12 ⁶School of Environmental Science and Engineering, Tianjin University, Tianjin, 300072, China

13 ⁷School of Environment and Natural Resources, Renmin University of China, Beijing, 100872, China

14 ⁸College of Urban and Environmental Sciences, Peking University, Beijing, 100871, China

15
16
17
18
19 *Correspondence to:* Qianggong Zhang (qianggong.zhang@itpcas.ac.cn) and Shichang Kang (shichang.kang@lzb.ac.cn)

24 **Abstract**

25 Total gaseous mercury (TGM) concentrations were continuously measured at the Nam Co Station, a remote high-altitude
26 site (4730 m a.s.l.), in the inland Tibetan Plateau, China from January 2012 to October 2014 using a Tekran 2537B instrument.
27 The mean concentration of TGM during the entire monitoring period was $1.33 \pm 0.24 \text{ ng m}^{-3}$ (mean \pm standard deviation (SD)),
28 ranking the lowest value among all continuous TGM measurements reported all over China, and was lower than most of sites
29 in the Northern Hemisphere. This indicated the pristine atmospheric environment in the inland Tibetan Plateau. Long-term
30 TGM at the Nam Co Station exhibited a slight decrease especially for summer seasons. The seasonal variation of TGM was
31 characterized by higher concentrations during warm seasons and lower concentrations during cold seasons, decreasing in the
32 following order: summer ($1.50 \pm 0.20 \text{ ng m}^{-3}$) > spring ($1.28 \pm 0.20 \text{ ng m}^{-3}$) > autumn ($1.22 \pm 0.17 \text{ ng m}^{-3}$) > winter ($1.14 \pm 0.18 \text{ ng}$
33 m^{-3}). Diurnal variations of TGM exhibited uniform patterns in different seasons: the daily maximum was reached in the
34 morning (around 2-4 hours after sunrise), followed by a decrease until sunset and a subsequent build-up at night, especially in
35 the summer and the spring. Regional surface re-emission and vertical mixing were two major contributors to the temporal
36 variations of TGM while long-range transported atmospheric mercury promoted elevated TGM during warm seasons. Results
37 of multiple linear regression (MLR) revealed that humidity and temperature were the principal covariates of TGM. Potential
38 source contribution function (PSCF) and FLEXible PARTicle dispersion model (WRF-FLEXPART) results indicated that the
39 likely high potential source regions of TGM to the Nam Co are central and eastern Indo-Gangetic Plain (IGP) during the
40 measurement period with high biomass burning and anthropogenic emissions. The seasonality of TGM at Nam Co was in
41 phase with the Indian Monsoon Index, implying Indian Summer Monsoon as an important driver for transboundary transport
42 of air pollution into the inland Tibetan Plateau. Our results provided atmospheric mercury baseline in the remote inland Tibetan
43 Plateau and serve as new constraint for assessment of Asian mercury emission and pollution.

44
45
46
47
48

49 **1 Introduction**

50 Mercury (Hg) is one of the most toxic environmental pollutant because of the easy uptake of its organic forms by biota
51 and the neurological and cardiovascular damage to humans resulting from bioaccumulation (Schroeder and Munthe, 1998).
52 The majority of the mercury released to the environment is emitted into the atmosphere and can be transported from emission
53 sources to deposition sites around the globe. Unlike other metals in the atmosphere, the majority of atmospheric mercury
54 largely exists in the elemental form (Gaseous Elemental Mercury, GEM). The global residence time of GEM is in the range of
55 0.5-2 years due to its high volatility, low solubility and chemical stability (Schroeder and Munthe, 1998; Shia et al., 1999). It
56 is therefore transported globally over long distances (tens of thousands of kilometers) far from pollution sources. Horowitz et
57 al. (2017) recently reported that the chemical lifetime of tropospheric GEM against oxidation may be much shorter than
58 previously reported: it could be as short as 2.7 months. GEM accounts for more than 95% of TGM (TGM, Total Gaseous
59 Mercury. RGM, Reactive Gaseous Mercury. TGM= GEM + RGM). RGM and Hg-P (particle-bound mercury) compounds
60 make up the remaining fraction of mercury in the atmosphere, and these two compounds have an estimated lifetime ranging
61 from several days to a few weeks. RGM can be expected to be removed near a few tens to a few hundreds of kilometers from
62 their source while Hg-P is likely to be deposited at intermediate distances of hundreds to thousands of kilometers (Schroeder
63 and Munthe, 1998). RGM and Hg-P are generally depicted as local and regional pollutants, and the dry and wet deposition of
64 RGM and Hg-P are much faster than GEM (Schroeder and Munthe, 1998; Lin and Pehkonen, 1999; Lindberg and Stratton,
65 1998).

66 East Asia and South Asia are two of the areas in the world with the fastest economic growth and the highest population
67 density. These two areas are known for their heavily polluted air (Nair et al., 2007; Mukherjee et al., 2009), and anthropogenic
68 mercury emissions in these areas are among the world's highest (Pirrone et al., 2010). China is the largest anthropogenic
69 emitter of mercury worldwide with most of the emissions originating from coal combustion and non-ferrous smelting
70 production (AMAP/UNEP, 2013; Pacyna et al, 2008). Geographically, most of China's mercury emissions are located in
71 eastern and central China (Streets et al., 2005; Wu et al., 2016) (Fig. S1). Atmospheric mercury concentrations in Guizhou,
72 one of the most important mercury producing and coal producing regions in China, was reported to be 6.2 - 9.7 ng m⁻³ of TGM
73 in the capital city of Guiyang between 2001- 2009 (Feng et al., 2004; Liu et al., 2011; Fu et al., 2011). Measurements of

74 atmospheric mercury at background and remote sites in China include the following sites: Wuzhishan (2011-2012), Mt.
75 Changbai (2008-2010), Mt. Waliguan (2007-2008), Mt. Ailao (2011-2012), Shangeri-La (2009-2010) and Mt. Gongga (2005-
76 2006) with concentrations ranging from 1.58 to 3.98 ng m⁻³ (Liu et al., 2016; Fu et al., 2012b; Fu et al., 2012a; Fu et al. 2015;
77 Zhang et al., 2015; Fu et al., 2008). Similarly, South Asia has serious problems of environmental pollution due to elevated
78 mercury emissions (UNEP, 2013), resulting in hazardous mercury levels reported in water, lake sediment and fish samples
79 (Karunasagar et al., 2006; Parvathi et al., 2010; Subramanian, 2004). Anthropogenic mercury emissions in South Asia were
80 mostly in the Indo-Gangetic Plain (IGP) including most of northern and eastern India, the eastern parts of Pakistan, and all of
81 Bangladesh (Fig. S1) all of which have high population density and many industrial centers. Biomass burning is another
82 important source of atmospheric mercury, especially for TGM/GEM (Pirrone et al., 2010), and can lead to high TGM
83 concentration events at sites far from the emissions (de Foy et al., 2012). Plenty of fire hot spots were observed in South Asia
84 and East Asia including the IGP, the Indo-China Peninsula and southeastern China indicating the biomass burning at these
85 areas (Fig. S2), while few biomass burning events were detected in the Tibetan Plateau (Fig. S2).

86 Located between South Asia and East Asia, the Tibetan Plateau is a vast high-altitude landform featured by remote and
87 pristine environments. There are limited local anthropogenic activities in the Tibetan Plateau and previous studies reported
88 that the atmospheric environment of the Tibetan Plateau remains global background levels (Fu et al., 2012a; Sheng et al., 2013;
89 Xiao et al., 2012). Notably, mercury records from glaciers and lake sediments suggest that the Tibetan Plateau is an important
90 part of the global mercury cycle, acting as both a sink (mercury deposition to snow) and a source (release of mercury from
91 melting ice) (e.g., Kang et al., 2016; Yang et al., 2010; Sun et al., 2017, Sun et al., 2018). Further, it has been increasingly
92 perceived that the inland of Tibetan Plateau can be influenced by trans-boundary air pollution such as black carbon originating
93 from biomass burning in South Asia by crossing the Himalayas (Xia et al., 2011; Cong et al., 2015; Wan et al., 2015; Li et al.,
94 2016). Studies of mercury in precipitation and water vapor evidenced that the Tibetan Plateau is likely sensitive to pollutant
95 input including mercury (Huang et al., 2012; Huang et al., 2013), and the particulate-bound mercury in total suspended
96 particulates was found at high concentrations in Lhasa with an average of 224 pg m⁻³ which was comparable to other cities in
97 China (Huang et al., 2016). A few measurements of atmospheric mercury at sites on the fringes of the Tibetan Plateau reported
98 TGM concentrations in the range of 1.98-3.98 ng m⁻³ (Fu et al., 2012a; Fu et al., 2008; Zhang et al., 2015), which were slightly

99 higher than the northern hemispherical background level, implying possible impact of anthropogenic emissions. In recent years,
100 China and India signed the Minamata Convention and will probably control mercury emissions more strictly (Selin, 2014).
101 Wu et al. (2017) stated that atmospheric mercury emissions from iron and steel production decreased from 35.6 Mg in 2013 to
102 32.7 Mg in 2015, and Pacyna et al. (2010) estimated that total mercury emissions in China would decrease from 635 Mg in
103 2005 to 290–380 Mg in 2020. Burger et al. (2013) estimated that total mercury emissions in India would increase from 310
104 Mg in 2010 to 540 Mg in 2020. In the context of serious mercury pollution and fast changes of regional mercury emission,
105 atmospheric mercury observations at background sites neighboring regions of higher mercury pollution can provide a scientific
106 basis for evaluating the extent of mercury pollution, for determining potential sources of atmospheric mercury and for
107 informing public policy. The Nam Co Station, an inland site in the Tibetan Plateau, is an ideal site to determine the TGM of
108 the inland Tibetan Plateau because it is rarely affected by locally anthropogenic emission of mercury.

109 In this study, high-time resolution TGM was measured at the Nam Co Station from January 2012 to October 2014 and
110 the temporal characteristics of atmospheric mercury were studied. Comparison with meteorological data, Multiple Linear
111 Regression (MLR) and a box model were used to investigate the temporal mercury variations at the Nam Co Station. HYSPLIT
112 (HYbrid Single-Particle Lagrangian Integrated Trajectory), WRF-FLEXPART (FLEXible PARTicle dispersion model) and
113 Potential Source Contribution Function (PSCF) were used to identify potential sources and impacts from long-range transport.
114 The objective of this study is to (1) summarize the levels and temporal characteristics of TGM at a remote site in the inland
115 Tibetan Plateau in a long-term measurement, (2) identify potential source regions of TGM at the Nam Co Station and (3)
116 provide in-situ observational constraint that may contribute to understand changes in Asian mercury pollution.

117 **2 Measurements and Methods**

118 **2.1 Measurement site**

119 The Nam Co comprehensive observation and research station (namely the Nam Co Station, 30°46.44' N, 90°59.31' E,
120 and 4730 m a.s.l.) is a remote site between Nam Co Lake and the Nyainqêntanglha mountain range (Fig. 1). The Nam Co
121 Station has been established since 2005 for maintaining a long-term record of the meteorological, ecological, and atmospheric
122 measurements in the Tibetan Plateau (Cong et al., 2007; Li et al., 2007; Kang et al., 2011; Huang et al., 2012; Liu et al., 2015;

123 de Foy et al., 2016b). There are restricted point sources of anthropogenic mercury emissions nearby the Nam Co Station.
124 Dangxiong County is the nearest town on the southern slopes of the Nyainqêntanglha mountain range approximately 60 km
125 south from Nam Co and Dangxiong is about 500 m lower than the Nam Co Station. Nomadism and tourism are the only human
126 activities mostly during summer. Lhasa, the largest city in Tibet, is ~125 km south of the Nam Co Station. There was snow at
127 the Nam Co Station discontinuously from October to March. But due to the strong wind at this period and the flat terrain
128 surrounding the station, the snow did not remain on the ground for more than a few days at a time.

129 TGM measurements were conducted at the Nam Co Station starting on January 15, 2012 until October 4, 2014 (Fig. S3).
130 Field operators checked the instruments and created a monitoring log file each day at the Nam Co Station. Measurements were
131 intermittently interrupted because of equipment maintenance and unstable power supply due to damage from strong winds to
132 the electrical wires at the Nam Co Station. All data displayed in this study are in UTC+8 and solar noon at the Nam Co Station
133 is at 13:56 in UTC+8 (China Standard Time, Beijing Time).

134 **2.2 Measurements: TGM, surface ozone and meteorology**

135 Measurements of TGM concentrations were performed with a Tekran model 2537 B instrument (Tekran Instruments
136 Corp., Toronto, Ontario, Canada). The Tekran 2537 B was installed in the monitoring house at the Nam Co Station and ambient
137 air was introduced from the inlet which was 1.5 m above the roof and 4 m above the ground. A 45-mm diameter Teflon filter
138 (pore size 0.2 μm) was placed in front of the inlet and it was changed every two weeks. The Tekran 2537 B measurements are
139 based on the amalgamation of mercury onto a pure gold surface. By using a dual cartridge design, continuous measurements
140 of mercury in the air can be made. The amalgamated mercury was thermally desorbed into an argon carrier gas stream and
141 analyzed using an internal detector which was designed by cold vapor atomic fluorescence spectrophotometry ($\lambda=253.7\text{nm}$)
142 (Landis et al., 2002) providing TGM analysis at sub-ng m^{-3} levels. The sampling interval of the Tekran 2537 B was 5 min and
143 the sampling flow rate was 0.8 L min^{-1} (at standard temperature and pressure). The Tekran 2537 B was calibrated automatically
144 every 25 hours using the internal mercury permeation source and was calibrated manually using a Tekran 2505 randomly 1-2
145 times a year. At the Nam Co Station, the TGM fraction consists mostly of GEM (more than 98%). The operationally defined
146 RGM accounted for less than 2% of TGM (Figure S1 in supplementary material in de Foy et al., 2016b). We consider the

147 Tekran data to represent TGM in line with previous studies (e.g. Kock et al., 2005; Slemr et al., 2008; Müller et al., 2012).

148 Surface ozone was measured as a surrogate measure of oxidizing potential of the atmosphere (Stamenkovic et al., 2007)
149 at the Nam Co Station using a UV photometric instrument (Thermo Environmental Instruments, USA, Model 49i) which uses
150 absorption of radiation at 254 nm and has a dual cell design. The monitor was calibrated using a 49i-PS calibrator (Thermo
151 Environmental Instruments, USA) before measurements and using aperiodic calibration during the monitoring periods. Details
152 and analysis of the surface ozone measurements at the Nam Co Station were reported in Yin et al. (2017).

153 Measurements of temperature (T), relative humidity (RH), wind speed (WS), wind direction (WD) and downward
154 shortwave radiation (SWD) were conducted at the Nam Co Station by a local weather station system (Milos 520, Vaisala Co.,
155 Finland) and a radiation measurement system (CNR1, Kipp & Zonen Co., US), respectively (Ma et al., 2008).

156 **2.3 Meteorological simulations**

157 Gridded meteorological data for backward trajectories were obtained from the Global Data Assimilation System (GDAS-
158 1) of the U.S. National Oceanic and Atmospheric Administration (NOAA) with $1^\circ \times 1^\circ$ latitude and longitude horizontal
159 resolution and vertical levels of 23 from 1000 hPa to 20 hPa (<http://www.arl.noaa.gov/gdas1.php>).

160 Backward trajectories and clusters were calculated using the NOAA-HYSPLIT model (Draxler and Rolph, 2003,
161 <http://ready.arl.noaa.gov/HYSPLIT.php>) using TrajStat (Wang et al., 2009), which is a free software plugin of MeteoInfo
162 (Wang, 2014). The backward trajectories arrival height in HYSPLIT was set at 500 m above the surface and the total run times
163 was 120 hours for each backward trajectory. Results of air masses at different heights (500m, 1000m and 1500m) showed
164 similar patterns, hence, we selected trajectories released at a height of 500 m as representative since 500 m is suitable for
165 considerations of both the long-range transport and transport in the planetary boundary layer. Trajectory positions were stored
166 at time intervals of 3 hours. Angular distance was chosen to calculate clusters in HYSPLIT calculation. HYSPLIT backward
167 trajectories were used to calculate the Potential Source Contribution Function (section 2.6) which serves to investigate the
168 potential sources contributing to atmospheric mercury at the Nam Co Station.

169 In addition to HYSPLIT, WRF-FLEXPART (Brioude et al., 2013) was used to obtain clusters of particle trajectories

170 reaching the Nam Co Station. 1000 particles were released per hour in the bottom 100 m surface layer above the Nam Co
171 Station and were tracked in backward mode for 4 days (de Foy et al., 2016b). The use of two different trajectory models
172 (HYSPLIT and WRF-FLEXPART) with different input meteorology can add robustness to the discussion as was done for the
173 ozone study at Nam Co (Yin et al., 2017). Furthermore, the WRF-FLEXPART simulations were some of the parameters used
174 in the multiple linear regression model (section 2.4). Residence Time Analysis (RTA) (Ashbaugh et al., 1985) was utilized to
175 show the dominant transport paths of air masses impacting the samples (Wang et al., 2016; Wang et al., 2017). Six clusters
176 were found to represent the prevailing flow patterns to the Nam Co Station simulated using WRF-FLEXPART.

177 **2.4 Multiple linear regression model and box model**

178 A Multiple Linear Regression (MLR) model was used to quantify the main factors affecting the hourly concentrations of
179 TGM. The method follows the description provided in de Foy et al. (2016a; 2016c) and de Foy (2017) and was used to analyze
180 surface ozone concentrations at the Nam Co Station (Yin et al., 2017). The inputs to the MLR model include meteorological
181 parameters (wind speed, temperature, solar radiation and humidity), surface ozone, inter-annual variation factors, seasonal
182 factors, diurnal factors, WRF boundary layer heights, WRF-FLEXPART trajectory clusters and a CAMx stratospheric ozone
183 tracer (see Yin et al. (2017) for more details). Briefly, the inter-annual factors are separate scaling factors for each year of the
184 measurements, the seasonal factors are 12-month and 6-month harmonic terms (sine and cosine), and the diurnal factors are
185 scaling factors for each hour of the day. The inputs to the model were normalized linearly. An Iteratively Reweighted Least
186 Squares (IRLS) procedure was used to screen for outliers. Measurement times when the model residual was greater than two
187 standard deviations of all the residuals were excluded from the analysis. This was repeated iteratively until the method
188 converged on a stable set of outliers. The variables to be included in the regression were obtained iteratively. At each iteration,
189 the variable leading to the greatest increase in the square of Pearson's correlation coefficient was added to the inputs as long
190 as the increase was greater than 0.005.

191 The distribution of TGM concentrations is approximately normal (see details in section 3.1), and so a linear model was
192 used. TGM was scaled linearly to have a mean of 0 and a standard deviation of 1 in the regression model. A Kolmogorov-
193 Zurbenko filter (Rao et al., 1997) was used to separate the time series of specific humidity and temperature into a synoptic

194 scale signal (> 3-5 days) and a diurnal scale signal using 5 passes of a 13-point moving average. Only the synoptic scale signal
195 was included in the final regression results, as the diurnal variation was characterized by the other variables in the analysis.
196 The other meteorological parameters used were the 24-hour average boundary layer height from WRF and the 8-hour local
197 measured wind speeds (4 directions, 5 wind speed segments for a total of 20 factors corresponding to different wind speeds
198 from different wind directions). The 24-hour average of ozone measurements (log-transformed) contributed to the model. In
199 addition, a seasonal K-Z filtered time series of a CAMx tracer for transport from the free troposphere (above 300 hPa) to the
200 surface contributed to the model.

201 TGM at the Nam Co Station is expected to be well mixed and the site is not influenced by local sources. It is therefore
202 expected that a box model should be able to reproduce the diurnal profile of concentrations. A box model that accurately
203 simulates the diurnal profile of TGM would provide constraints on known processes affecting the concentrations. Comparisons
204 with measured profiles would further identify missing processes in the model. This approach was used for reactive mercury at
205 the same site, where it identified the role of the reduction of reactive mercury to gaseous elementary mercury mediated by
206 sunlight (de Foy et al., 2016b). A box model was made that included free parameters to represent known chemical reactions
207 and dispersion processes. An optimization algorithm was used to identify the parameters required to fit the model to the data,
208 as was done in de Foy et al. (2016b). Preliminary tests of the box model were made using solar radiation and temperature to
209 represent chemical transformations, as well as using wind speed and boundary layer height to represent dilution. However
210 these attempts failed to reproduce the diurnal variation found in the measurements. A simplified exploratory model was
211 therefore sought that would represent the measured diurnal variations as simply as possible, according to Occam's razor
212 (Larsen et al., 2014). Although this model does not yield direct information on known processes, it does identify the kinds of
213 processes and their magnitude that would be required to accurately represent the measured diurnal profile. The final model
214 combined the following 5 inputs: TGM increases at sunrise and in the early evening, constant TGM reductions 24 hours a day,
215 a constant lifetime for TGM loss during daylight hours and TGM dilution due to vertical mixing.

216 **2.5 Anthropogenic mercury emissions and fire hot spots distribution**

217 The mercury emission inventory of China was obtained from Wu et al. (2016), which used a technology-based approach
218 to compile a comprehensive estimate of Chinese provincial emissions for all primary anthropogenic sources. The emissions

219 over other Asian countries were from UNEP global anthropogenic emission inventory (AMAP/UNEP, 2013). These
220 inventories were for the year 2010 and had a horizontal resolution of $0.5^{\circ} \times 0.5^{\circ}$.

221 MODIS fire spots were obtained from Fire Information for Resource Management System (FIRMS) operated by the
222 National Aeronautics and Space Administration (NASA) of the United States (Giglio et al., 2003; Davies et al., 2004).

223 **2.6 Potential Source Contribution Function (PSCF)**

224 PSCF assumes that back-trajectories arriving at times of higher mixing ratios likely point to the more significant source
225 directions (Ashbaugh et al., 1985). PSCF has been applied in previous studies to locate sources of TGM for different sites (Fu
226 et al., 2012a; Fu et al., 2012b; Zhang et al., 2015). The PSCF values for the grid cells in the study domain are based on a count
227 of the trajectory segment (hourly trajectory positions) that terminate within each cell (Ashbaugh et al., 1985). Let n_{ij} be the
228 total number of endpoints that fall in the ij th cell during whole simulation period. Let m_{ij} represents the number of points in
229 the same cell that have arrival times at the sampling site corresponding to TGM concentrations higher than a set criterion. In
230 this study, we calculate the PSCF based on trajectories corresponding to concentrations that exceed the mean level (1.33 ng m^{-3})
231 of TGM. The PSCF value for the ij th cell is then defined as:

$$232 \text{PSCF}_{ij} = m_{ij}/n_{ij}$$

233 The PSCF value can be interpreted as the conditional probability that the TGM concentration at measurement site is
234 greater than the mean mixing ratios if the air parcel passes through the ij th cell before arriving at the measurement site. In cells
235 with high PSCF values are associated with the arrival of air parcels at the receptor site that have TGM concentrations that
236 exceed the criterion value. These cells are indicative of areas of 'high potential' contributions for the chemical constituent.

237 Identical PSCF_{ij} values can be obtained from cells with very different counts of back-trajectory points (e.g. grid cell A
238 with $m_{ij}=5000$ and $n_{ij}=10000$ and grid cell B with $m_{ij} = 5$ and $n_{ij} = 10$). In this extreme situation grid cell A has 1000 times
239 more air parcels passing through than grid cell B. Because of the sparse particle count in grid cell B, the PSCF values are more
240 uncertain and the contribution from B is limited. To account for the uncertainty due to low values of n_{ij} , the PSCF values were
241 scaled by a weighting function W_{ij} (Polissar et al., 1999). The weighting function reduced the PSCF values when the total
242 number of the endpoints in a cell was less than about three times the average value of the end points per each cell. In this case,

243 W_{ij} was set as follows:

$$244 \quad W_{ij} = \begin{cases} 1.00 & n_{ij} > 3N_{ave} \\ 0.70 & 3N_{ave} > n_{ij} > 1.5N_{ave} \\ 0.42 & 1.5N_{ave} > n_{ij} > N_{ave} \\ 0.05 & N_{ave} > n_{ij} \end{cases} \quad (1)$$

245 where N_{ave} represents the mean n_{ij} of all grid cells. The weighted PSCF values obtained by multiplying the original PSCF
246 values by the weighting factor: weighted PSCF result= W_{ij} ×PSCF.

247 **3 Results and discussion**

248 **3.1 TGM concentrations**

249 The mean TGM concentration at the Nam Co Station is $1.33 \pm 0.24 \text{ ng m}^{-3}$, which is the lowest among all reported TGM
250 concentrations at remote and rural sites in China (Liu et al., 2016; Fu et al., 2012b; Fu et al., 2012a; Fu et al. 2015; Ci et al.,
251 2011; Dou et al., 2013; Zhang et al., 2015; Fu et al., 2010; Li et al., 2011; Zhang et al., 2013; Yu et al., 2015; Fu et al., 2008;
252 Chen et al., 2013). The mean concentration of TGM is slightly lower than the annual mean concentration at background sites
253 in the Northern Hemisphere (1.55 ng m^{-3} in 2013 and 1.51 ng m^{-3} in 2014), and higher than those in the Southern Hemisphere
254 (0.93 ng m^{-3} in 2013 and 0.97 ng m^{-3} in 2014) (Sprovieri et al., 2016). Comparable results were reported from EvK2CNR on
255 the south slope of the Himalayas (1.2 ng m^{-3} , Gratz et al., 2013), and from tropical sites in the Global Mercury Observation
256 System in the Northern Hemisphere (1.23 ng m^{-3} in 2013 and 1.22 ng m^{-3} in 2014) (Sprovieri et al., 2016). Comparing to the
257 three sites at the edge of the Tibetan Plateau (Mt. Waliguan, Shangri-La and Mt. Gongga, Table S1), the mean TGM
258 concentration at the Nam Co Station was substantially lower, indicating that the inland Tibetan Plateau has a more pristine
259 environment than the edges of the plateau.

260 The frequency distribution of TGM at the Nam Co Station was normally distributed (Fig. S4). 81% of hourly average
261 TGM concentrations were in the range of $1.0\text{-}1.6 \text{ ng m}^{-3}$ with few episodically elevated TGM and low TGM concentrations.
262 1.6% ($n=236$) out of all hourly mean TGM data ($n=14408$) were greater than 1.81 ng m^{-3} (overall mean TGM + $2 \times \text{SD}$, namely
263 $1.33 + 2 \times 0.24 = 1.81$), and 1.5% ($n=213$) were lower than 0.85 ng m^{-3} (overall mean TGM - $2 \times \text{SD}$, namely $1.33 - 2 \times 0.24 = 0.85$).

264 The monthly average TGM at the Nam Co Station showed a weak decrease (slope = -0.006) during the entire monitoring
265 period, and the decrease was more pronounced in the summer (slope = -0.013). Despite the short time span of the TGM time

266 series with some missing data mostly in the winter, the slight decrease of TGM especially in the summer was in agreement
267 with a recent study using plant biomonitoring which identified a decreasing atmospheric mercury since 2010 near Dangxiang
268 county (Tong et al., 2016) as well as decreases of TGM at other sites (Slemr et al., 2011; Zhang et al., 2016).

269 **3.2 Seasonal variations of TGM**

270 In contrast with many previous observations in China (Zhang et al., 2015; Fu et al., 2008b; Fu et al., 2009; Fu et al., 2010;
271 Fu et al., 2011; Fu et al., 2012b; Feng et al., 2004; Xiu et al., 2009; Xu et al., 2015; Wan et al., 2009) and most AMNet
272 (Atmospheric Mercury Network) sites (Lan et al., 2012), TGM at the Nam Co Station showed a seasonal variation with a
273 maximum in the summer (June, July and August) and a minimum in the winter (December, January and February) (Fig. 2).
274 The seasonal mean TGM values decreased in the following order: summer ($1.50 \pm 0.20 \text{ ng m}^{-3}$) > spring ($1.28 \pm 0.20 \text{ ng m}^{-3}$) >
275 autumn ($1.22 \pm 0.17 \text{ ng m}^{-3}$) > winter ($1.14 \pm 0.18 \text{ ng m}^{-3}$) (Table 1). The highest monthly mean TGM concentration of 1.54 ng
276 m^{-3} in July was 0.43 ng m^{-3} higher than the lowest of 1.11 ng m^{-3} in November.

277 Measurements of TGM in other sites in the Tibetan Plateau also reported diverse seasonal patterns (Fig. 3). For example,
278 Fu et al. (2012a) found that at Waliguan the maximum TGM concentration was in January 2008, resulting from long-range
279 transport of pollutions from Northern India. Aside from January, monthly mean TGM concentrations at Waliguan had a clear
280 trend with high levels in warm seasons, and lower levels in cold seasons. The TGM variation at Mt. Gongga (Fu et al., 2008)
281 had a minimum in the summer, possibly due to the accelerated oxidation followed by dry deposition and wet scavenging
282 processes in the summer. The winter maximum of TGM at Mt. Gongga (Fu et al., 2008) implied the impact from anthropogenic
283 mercury emissions in the cold months. The seasonal variation of TGM at Shangri-La (Zhang et al., 2015) had high levels in
284 the spring and autumn, and low levels in the summer and winter which was different from all the other sites in the Tibetan
285 Plateau.

286 Compared to other high-altitude background sites in the mid-latitudes in Europe (Fig. 4) (Denzler et al., 2017; Fu et al.,
287 2016a; Ebinghaus et al., 2002) and sites in mid-latitudes in the US (Holmes et al., 2010; Weiss-Penzias et al., 2003; Sigler et
288 al., 2009; Yatavelli et al., 2006), the lower concentration of TGM at the Nam Co Station in the winter might be indicative of
289 atmospheric mercury removal in the winter caused by reactive halogens (Br and Br₂). The reaction rates for these reactions are
290 a strong inverse function of temperature (de Foy et al., 2016b; Goodsite et al., 2004), and they are accompanied by lower

291 surface ozone concentration (Yin et al., 2017), which is catalytically destroyed by halogens (Bottenheim et al., 1986; Obrist et
292 al., 2011).

293 The summer peak of TGM at the Nam Co Station may be related to both the local re-emission of mercury from the earth's
294 surface, and the long-range transport of mercury from South Asia (see details in section 3.5). At the Nam Co Station, daily
295 mean TGM had a correlation coefficient with daily mean temperature reaching 0.56. Higher temperature in the warm seasons
296 (Fig. 5) might lead to remobilization of soil mercury re-emission, which has been evidenced by a recent study on surface-air
297 mercury exchange in the northern Tibetan Plateau (Ci et al., 2016). It is also possible that weaker wind speeds during the warm
298 season (Fig. 5) suppressed the dilution of TGM with fresh air aloft in a low boundary layer. Furthermore, most precipitation
299 happens in the summer at the Nam Co Station (You et al., 2007) and can increase emission of mercury from the Earth's surface
300 by physical displacement of interstitial soil air by the infiltrating water (Ci et al., 2016) and by additional input of mercury
301 from wet deposition (Huang et al., 2012). Besides local emissions, the summer monsoon can facilitate the transport of air
302 masses with higher TGM concentrations from South Asia, and hence may also contribute to the summer peak of TGM.

303 The month of April in both 2012 and 2013 had higher monthly TGM levels than the months before and after (Fig. S3),
304 possibly resulting from mercury emission from Nam Co Lake as the lake started to thaw in April (Gou et al., 2015).

305 **3.3 Diurnal variations of TGM**

306 Diurnal variations of TGM in different seasons exhibited a regular pattern, characterized by a sharp rise shortly after
307 sunrise and a fairly steady decrease from the morning peak until sunset (Fig. 6). After sunset, TGM increased until midnight
308 in the summer, the spring and the autumn. The diurnal variation of TGM at the Nam Co Station was similar to those of Mt.
309 Gongga (Fu et al., 2009), Mt. Leigong (Fu et al., 2010), Mt. Changbai (Fu et al., 2012b), Mt. Waliguan (Fu et al., 2012a) and
310 Reno (Peterson et al., 2009) except that the morning increase occurs earlier and is shorter compared during other sites that
311 have a gradual increase throughout the morning.

312 Fig. 7 showed the comparison of TGM concentrations with a box model simulation by seasons. The best match in the box
313 model was obtained by using variables including constant TGM reduction throughout the day, TGM increases at sunrise, TGM
314 increases in the early evening, TGM dilution due to vertical mixing and a lifetime of TGM loss during daylight hours (Table
315 2). The R^2 of the model simulation ranged from 0.91 to 0.99, suggesting that the simulations reproduced the diurnal variations

316 accurately. As described above, both the measurements and the model have sharp bursts of TGM in the morning (7:00-9:00)
317 and in the evening (18:00-22:00) during all seasons. Constant reductions existed in the spring, summer and autumn which
318 would correspond to reduction rates of around 1 to 2 ng m⁻² h⁻¹.

319 Fig. 8 showed the seasonal diurnal profiles of TGM and meteorological parameters. TGM concentrations were stable or
320 slightly decreasing after midnight (0:00-6:00) under shallow nocturnal boundary layers. Notably, the morning increase of TGM
321 happens immediately after sunrise, but before the increases of temperature, wind speed or humidity. The atmospheric mercury
322 bursts in the morning (7:00-9:00) is probably due to prompt re-emission of nocturnal mercury deposition on the Earth's surface
323 (Fu et al., 2016b; Howard et al., 2017; Kim 2010). The stable nocturnal boundary layer terminated at sunrise at which point
324 mercury, including the mercury in the soil indigenously and/or deposited overnight, started to be reemitted into the shallow
325 stable boundary layer before the increase of temperature which leads to an increase in the mixing height. As the temperature
326 and radiation increased, so did the boundary layer height which developed into a convective mixed boundary layer and
327 generated greater vertical mixing between the surface and loft. At the same time, the surface wind speed also increased. With
328 increased vertical and horizontal dispersion, TGM released from the surface was diluted during the daytime (Liu et al., 2011;
329 Lee et al., 1998). When the temperature decreased and the boundary layer converted back into a nocturnal boundary layer after
330 sunset, depressed vertical mixing facilitated the build-up of TGM and such build-up was more significant in the warm seasons.
331 In the evening, increases in TGM correspond to increases in specific humidity, especially in the summer.

332 **3.4 Multiple linear regression and WRF-FLEXPART clusters results**

333 Results of the MLR simulations for the entire measurement period (2012-2014) had a close correlation with the
334 measurements: the correlation coefficient was 0.77 for all 12649 data points and 0.84 excluding the 383 outliers (Fig. 9). The
335 primary contributor to the variance of the simulated time series was the seasonal signal, including the 12-month and 6-month
336 harmonics as well as the smoothed specific humidity and temperature time series (Table 3). These were grouped together when
337 presenting the results because they were not orthogonal to each other, and they contributed 84% of the variance of TGM in
338 MLR simulation. The diurnal factors accounted for 4% of the variance, the WRF boundary layer heights accounted for 4% of
339 the variance, and the local winds were associated with 1% of the variance. These factors showed that there was an impact from
340 horizontal and vertical dispersion as well as daily cycling patterns due to either transport or chemistry, but that these factors

341 were considerably smaller than the seasonal variation at the site. Only 1% of the variance was associated with the annual signal,
342 showing that the decrease in the concentrations reported in Sec. 3.1 was a small contributor to variations in TGM at Nam Co.
343 The time series of surface ozone concentration contributed 3% to the variance and the stratospheric ozone tracer contributed
344 3%. We hypothesized that this was because ozone concentrations acted as an indicator of the oxidative potential of the air mass,
345 although in the case of surface ozone concentration it could also be because they were a tracer of aged polluted air masses.

346 The regression analysis screens for high and low outliers. In particular, high outliers were significant in terms of TGM
347 concentrations: they had an average concentration of 1.91 ng m^{-3} which is 0.58 ng m^{-3} higher than the average of the
348 measurements retained in the simulations (Fig. 9). Fig. 9 showed that a number of the high outliers are associated with specific
349 peak events, indicating that occasional plumes of high TGM are not associated with recurring emissions or periodically
350 occurring conditions. A significant amount of TGM not accounted-for in the model was due to the high outliers. Additionally,
351 a few events with very low TGM concentrations were not simulated. They have an average concentration of 0.9 ng m^{-3} . Fig.
352 10a showed the 6 wind transport clusters based on the hourly WRF-FLEXPART simulations. The figure showed the average
353 residence time analysis for all the hours in each cluster, which characterizes the path of the air masses arriving at the
354 measurement site for each cluster. The most frequent clusters were clusters 1 and 2 which accounted for 30% and 34% of
355 measurement hours respectively. For measurement times during these clusters, the air masses clearly came from the west with
356 a slight southern component for cluster 1 and a slight northern component in the case of cluster 2. Cluster 3 represented hours
357 influenced by transport from the north which occurred during 15% of the measurement period. These were associated with the
358 passage of storms at Nam Co: as the low pressure system moved to the east, the winds shifted from northwesterly to
359 northeasterly. Clusters 4, 5 and 6 occurred less frequently and all represented different types of wind transport across the
360 Himalayas from the south. Cluster 4 was the least frequent cluster, occurring 5% of the time. It included transport from the
361 southeast including the northeastern corner of the Indo-Gangetic plain and occasional transport from southwestern China. This
362 cluster also included transport from the direction of Lhasa. Cluster 5 occurred 7% of the time and represents transport from
363 the south including Bangladesh. Cluster 6 occurred 9% of the time and included transport from Nepal and northern India.

364 The WRF-FLEXPART clusters were included in the MLR analysis and helped to improve the simulations for several
365 tests. However, they did not increase the correlation coefficient of the final regression time series and consequently were not

366 included in the final MLR results. This could be because transport was already characterized by the other variables in the
367 model such as temperature and humidity (which can serve as tracers of different air masses) and local wind speed and direction.
368 Nevertheless, the importance of air mass transport can be seen from the probability density function of the TGM concentrations
369 by cluster shown in Fig. 10b. Clusters 1 and 2, which had transport from the west, clearly had the lowest TGM concentrations.
370 Next in terms of increasing TGM concentrations were clusters 3 and 6 which had transport from the north and from the
371 southwest. TGM concentrations above 2 ng m^{-3} are very clearly associated with cluster 4 which has transport from the east
372 and through Lhasa, which was also probably due to the further impact from eastern Indo-Gangetic Plain and the possibility of
373 episodic transport events from China. Of the 87 hours with concentrations higher than 2 ng m^{-3} , 59% occurred during cluster
374 4 and 17% during cluster 5 with less than 8% for each of the other clusters. This demonstrated clearly that in addition to having
375 the highest average levels, clusters 4 and 5 accounted for most of the peak concentrations.

376 **3.5 HYSPLIT and PSCF results**

377 Backward trajectories were calculated using HYSPLIT to identify the origins of air masses and associated TGM
378 concentrations to the Nam Co Station. Most HYSPLIT trajectories originated from the west of Nam Co including the western
379 and central Tibetan Plateau, the southwestern part of the Xinjiang Uygur Autonomous Region, South Asia, Central Asia and
380 Western Asia. Very few trajectories originated from eastern China (Fig. S5). The backward trajectories were grouped into 6
381 clusters. Cluster 3 indicated the air mass from the south, originating from Bhutan and Bangladesh. This cluster had the lowest
382 starting heights as well as traveling heights, but the highest mean TGM concentration (1.48 ng m^{-3}) (Table S2) in agreement
383 with the FLEXPART results (Sec. 3.4). Clusters 1, 2, 4, 5 and 6 originated in the west, including air masses originating from
384 northern India, Pakistan, Afghanistan and Iran passed over the Himalayas before arriving at the Nam Co Station. They had
385 longer pathways through the Tibetan Plateau than Cluster 3. Cluster 4 had the longest transport route from the west, suggestive
386 of faster wind speeds, and also the lowest TGM mean concentration (1.12 ng m^{-3}) with relatively high transport height.

387 PSCF calculations were based on concurrent TGM measurements and HYSPLIT backward trajectories, and thus can
388 further constrain the potential source regions. Areas including IGP, the southern part of the Xinjiang Uygur Autonomous
389 Region, the western part of Qinghai province and areas near the Nam Co Station in the Tibet Autonomous Region were
390 identified as overall high potential sources regions and pathways (Fig. S6). Except for the areas near the Nam Co Station, these

391 potential sources regions correspond well with the atmospheric mercury emissions and biomass burning. The Bay of Bengal
392 was identified as a potential source region probably due to high emissions from its surroundings associated with frequent
393 occurrence of trajectories passing through this area in the summer.

394 Seasonal PSCFs were calculated in 2012 to investigate the potential sources by seasons (Fig. 11). In the spring, the autumn
395 and the winter, the Nam Co Station was dominated by the Westerlies. Pollutants from South Asia might be diluted by the clean
396 air during the transport within the Tibetan Plateau before they arrived at the Nam Co Station (Fig. S7). A zonal region in the
397 central IGP (Fig. 11) with elevated pollution represents a constant potential source (Gautam et al., 2011; Mallik and Lal, 2014).
398 The significant impact of long-range transport pollution from northwestern India on the Tibetan Plateau was also evidenced
399 by TGM measurements at Waliguan (Fu et al., 2012a). In the summer, the Indian Monsoon prevails and air masses arrived at
400 the Nam Co Station that had shorter pathway after entering the Tibetan Plateau than those in other seasons (Fig. S7). The
401 central IGP was again found to have higher PSCF values than other regions, even though these were much lower than the
402 PSCF values of other seasons. The highest PSCF values in the summer were in the eastern IGP (Fig. 11). For all seasons, the
403 region near the Nam Co Station, especially its south and west, was high in PSCF values all through the year, indicating that
404 air masses with high TGM concentrations predominantly came from the south-southwest.

405 **3.6 Implications for transboundary air pollution to the Tibetan Plateau**

406 The seasonal atmospheric circulation pattern in the Tibetan Plateau was characterized by the Indian monsoon in the
407 summer and the Westerlies in the winter. Such a climate regime exerted a profound impact on the seasonal atmospheric
408 environment by affecting the air transport dynamic and associated climate conditions. Pollutants like black carbon and
409 hexachlorocyclohexanes peaked in pre-monsoon season and declined during monsoon season at Nam Co and Lulang, resulting
410 from seasonal rainfall variations that can scavenge aerosols during their transport from source regions to the Tibetan Plateau
411 (Zhang et al., 2017; Wan et al., 2015; Sheng et al., 2013). In contrast, gaseous pollutants showed different seasonal patterns:
412 TGM at Nam Co in this study and persistent organic pollutants (dichlorodiphenyltrichloroethane and polychlorinated biphenyls)
413 at Lulang showed higher concentrations during the monsoon season compared to the pre-monsoon season (Sheng et al., 2013).
414 TGM at Nam Co showed strong covariance with temperature and specific humidity, all of which are in phase with the Indian
415 Monsoon Index (IMI) (Wang and Fan, 1999; Wang et al., 2001) (Fig. 12), indicating the importance of Indian Summer

416 Monsoon as a major driver delivering of transboundary transport of air pollution into the inland Tibetan Plateau. We suggested
417 that gaseous pollutants were not readily deposited and/or washed out by precipitation during their transport and were more
418 likely associated with the transport dynamics driven by the Indian Summer Monsoon, hence they showed high values when
419 the Indian Summer Monsoon prevails. Transboundary air pollution was not the sole factor contributing to elevated TGM during
420 summer: temperature-dependent processes such as gas-particle fractionation and surface reemission can also contribute to such
421 seasonal patterns. Nonetheless, the close relationship between TGM and the Indian Summer Monsoon and the clear difference
422 in seasonal patterns between gaseous and particulate pollutants together indicated that additional measurements of multiple
423 pollutants and comparative studies are required to achieve a more comprehensive understanding and assessment of
424 transboundary air pollution to the Tibetan Plateau.

425 **4 Conclusions**

426 We conducted three-years of TGM measurements at the Nam Co Station in the inland area of the Tibetan Plateau, China,
427 from January 2012 to October 2014. The mean TGM concentration was 1.33 ± 0.24 ng m⁻³ during the whole measurement
428 period and the low TGM level at the Nam Co Station indicated that the environment is pristine in the inland Tibetan Plateau.
429 A weak decrease of TGM was identified over the course of the measurements.

430 In contrast to many other sites in China, TGM at the Nam Co Station showed high concentrations in warm seasons and
431 low concentrations in cold seasons. Compared with other high-altitude background sites, the low concentration of TGM at the
432 Nam Co Station in the winter may be due to the removal of mercury due to halogen. Seasonal variation of TGM at the Nam
433 Co Station was influenced by factors such as re-emission processes of deposited mercury over the Earth's surfaces, vertical
434 mixing and long-range transport. Multiple linear regression, backward trajectories and PSCF were investigated at the Nam Co
435 Station and results indicated that long-range transports from the central and eastern Indo-Gangetic Plain were potentially the
436 main sources for seasonally elevated TGM at the Nam Co Station due to the alternate impact of the Westerlies and of the Indian
437 monsoon. Peak concentrations of TGM at the Nam Co Station were associated with air masses from the eastern Indo-Gangetic
438 Plain with the possibility of episodic transport events from China.

439 At the Nam Co Station, the diurnal TGM profile had a peak 2-3 hours after sunrise and reached its lowest concentration
440 before sunset. An exploratory box model simulation shows that this diurnal profile can be accurately represented using TGM

441 reductions 24 hours per day, TGM increases near sunrise and sunset, and dilution due to vertical mixing. Daily meteorology
442 conditions, such as high temperature, high solar radiation and more precipitation facilitated the Earth's surface mercury
443 emission. The decline of TGM concentrations in the daytime was likely due to vertical dilution from increased vertical mixing,
444 as well as due to the conversion of GEM to oxidized species that are easily deposited.

445 Due to the insolubility of TGM, which is different from particulate pollutant, TGM was less affected by the precipitation
446 during the transport in monsoon season and measurement of TGM at the Nam Co Station can continually reflect the
447 transboundary air pollution from the South Asia to the inland Tibetan Plateau.

448 The measurements of TGM at the Nam Co Station will be useful in providing atmospheric mercury baseline in the remote
449 inland Tibetan Plateau, improving the accuracy of modeled concentrations of TGM in the inland Tibetan Plateau, and serving
450 as new constraint for assessment of Asian mercury emission and pollution.

451
452 Data availability. All the data presented in this paper can be made available for scientific purposes upon request to the
453 corresponding authors (Qianggong Zhang (qianggong.zhang@itpcas.ac.cn) or Shichang Kang (shichang.kang@lzb.ac.cn)).
454

455 **Acknowledgements**

456 This study was supported by the National Natural Science Foundation of China (41630754 and 41630748) and Q. G.
457 Zhang acknowledges financial support from the Youth Innovation Promotion Association of CAS (2016070). X. F. Yin
458 acknowledges China Scholarship Council. The authors are grateful to Yaqiang Wang, who is the developer of MeteoInfo and
459 who provided generous help. The authors thank NOAA for providing the HYSPLIT model and GFS meteorological files.
460 Finally, the authors would like to thank the editor and referees of this paper for their helpful comments and suggestions.

461
462
463
464
465

466 **References:**

- 467 AMAP/UNEP: Technical Background Report for the Global Mercury Assessment 2013, Arctic Monitoring and
468 Assessment Programme, 2013.
- 469 Ashbaugh, L. L., Malm, W. C., and Sadeh, W. Z.: A residence time probability analysis of sulfur concentrations at
470 Grand Canyon National Park, Atmospheric Environment (1967), 19, 1263-1270, 1985.
- 471 Assessment, U. G. M.: Sources, Emissions, Releases and Environmental Transport, UNEP Chemicals Branch, Geneva,
472 Switzerland, 42, 2013.
- 473 Bottenheim, J., Gallant, A. G., and Brice, K. A.: Measurements of NO_y species and O₃ at 82 N latitude, Geophysical
474 Research Letters, 13, 113-116, 1986.
- 475 Brioude, J., Arnold, D., Stohl, A., Cassiani, M., Morton, D., Seibert, P., Angevine, W., Evan, S., Dingwell, A., and Fast,
476 J. D.: The Lagrangian particle dispersion model FLEXPART-WRF version 3.1, Geoscientific Model Development, 6, 1889-
477 1904, 2013.
- 478 Burger Chakraborty, L., Qureshi, A., Vadenbo, C., and Hellweg, S.: Anthropogenic mercury flows in India and impacts
479 of emission controls, Environmental science & technology, 47, 8105-8113, 2013.
- 480 Chen, L., Liu, M., Xu, Z., Fan, R., Tao, J., Chen, D., Zhang, D., Xie, D., and Sun, J.: Variation trends and influencing
481 factors of total gaseous mercury in the Pearl River Delta—A highly industrialised region in South China influenced by
482 seasonal monsoons, Atmospheric environment, 77, 757-766, 2013.
- 483 Choi, H.-D., and Holsen, T. M.: Gaseous mercury emissions from unsterilized and sterilized soils: the effect of
484 temperature and UV radiation, Environmental Pollution, 157, 1673-1678, 2009.
- 485 Ci, Z., Peng, F., Xue, X., and Zhang, X.: Air–surface exchange of gaseous mercury over permafrost soil: an
486 investigation at a high-altitude (4700 m asl) and remote site in the central Qinghai–Tibet Plateau, Atmospheric Chemistry
487 and Physics, 16, 14741-14754, 2016.
- 488 Ci, Z., Zhang, X., Wang, Z., and Niu, Z.: Atmospheric gaseous elemental mercury (GEM) over a coastal/rural site
489 downwind of East China: temporal variation and long-range transport, Atmospheric environment, 45, 2480-2487, 2011.
- 490 Cong, Z., Kang, S., Liu, X., and Wang, G.: Elemental composition of aerosol in the Nam Co region, Tibetan Plateau,
491 during summer monsoon season, Atmospheric Environment, 41, 1180-1187, 2007.
- 492 Cong, Z., Kawamura, K., Kang, S., and Fu, P.: Penetration of biomass-burning emissions from South Asia through the
493 Himalayas: new insights from atmospheric organic acids, Scientific reports, 5, 9580, 2015.
- 494 Davies, D., Kumar, S., and Descloitres, J.: Global Fire Monitoring Use of MODIS Near-real-time Satellite Data, GIM
495 INTERNATIONAL, 18, 41-43, 2004.
- 496 Dou, H., Wang, S., Wang, L., Zhang, L., and Hao, J.: Characteristics of total gaseous mercury concentrations at a rural
497 site of Yangtze Delta, China, Huan jing ke xue= Huanjing kexue, 34, 1-7, 2013.
- 498 de Foy, B., Wiedinmyer, C., and Schauer, J.: Estimation of mercury emissions from forest fires, lakes, regional and
499 local sources using measurements in Milwaukee and an inverse method, Atmospheric Chemistry and Physics, 12, 8993-
500 9011, 2012.
- 501 de Foy, B., Lu, Z., and Streets, D. G.: Impacts of control strategies, the great recession and weekday variations on NO₂
502 columns above North American cities, Atmospheric Environment, 138, 74-86, 2016a.

503 de Foy, B., Tong, Y., Yin, X., Zhang, W., Kang, S., Zhang, Q., Zhang, G., Wang, X., and Schauer, J. J.: First field-
504 based atmospheric observation of the reduction of reactive mercury driven by sunlight, *Atmospheric Environment*, 134, 27-
505 39, 2016b.

506 de Foy, B., Lu, Z., and Streets, D. G.: Satellite NO₂ retrievals suggest China has exceeded its NO_x reduction goals
507 from the twelfth Five-Year Plan, *Scientific reports*, 6, 35912, 2016c.

508 de Foy, B.: City-level variations in NO_x emissions derived from hourly monitoring data in Chicago, *Atmospheric*
509 *Environment*, 2017.

510 Denzler, B., Bogdal, C., Henne, S., Obrist, D., Steinbacher, M., and Hungerbühler, K.: Inversion Approach to Validate
511 Mercury Emissions Based on Background Air Monitoring at the High Altitude Research Station Jungfraujoch (3580 m),
512 *Environmental Science & Technology*, 51, 2846-2853, 2017.

513 Draxler, R. R., and Rolph, G.: HYSPLIT (HYbrid Single-Particle Lagrangian Integrated Trajectory) model access via
514 NOAA ARL READY website (<http://www.arl.noaa.gov/ready/hysplit4.html>). NOAA Air Resources Laboratory, Silver
515 Spring, in, Md, 2003.

516 Ebinghaus, R., Kock, H., Coggins, A., Spain, T., Jennings, S., and, and Temme, C.: Long-term measurements of
517 atmospheric mercury at Mace Head, Irish west coast, between 1995 and 2001, *Atmospheric Environment*, 36, 5267-5276,
518 2002.

519 Feng, X., Tang, S., Shang, L., Yan, H., Sommar, J., and Lindqvist, O.: Total gaseous mercury in the atmosphere of
520 Guiyang, PR China, *Science of the Total Environment*, 304, 61-72, 2003.

521 Feng, X., Shang, L., Wang, S., Tang, S., and Zheng, W.: Temporal variation of total gaseous mercury in the air of
522 Guiyang, China, *Journal of Geophysical Research: Atmospheres*, 109, 2004.

523 Fu, X., Feng, X., Zhu, W., Wang, S., and Lu, J.: Total gaseous mercury concentrations in ambient air in the eastern
524 slope of Mt. Gongga, South-Eastern fringe of the Tibetan plateau, China, *Atmospheric Environment*, 42, 970-979, 2008.

525 Fu, X., Feng, X., Wang, S., Rothenberg, S., Shang, L., Li, Z., and Qiu, G.: Temporal and spatial distributions of total
526 gaseous mercury concentrations in ambient air in a mountainous area in southwestern China: Implications for industrial and
527 domestic mercury emissions in remote areas in China, *Science of the total environment*, 407, 2306-2314, 2009.

528 Fu, X., Feng, X., Dong, Z., Yin, R., Wang, J., Yang, Z., and Zhang, H.: Atmospheric gaseous elemental mercury
529 (GEM) concentrations and mercury depositions at a high-altitude mountain peak in south China, *Atmospheric Chemistry and*
530 *Physics*, 10, 2425-2437, 2010.

531 Fu, X., Feng, X., Qiu, G., Shang, L., and Zhang, H.: Speciated atmospheric mercury and its potential source in Guiyang,
532 China, *Atmospheric environment*, 45, 4205-4212, 2011.

533 Fu, X., Feng, X., Liang, P., Zhang, H., Ji, J., and Liu, P.: Temporal trend and sources of speciated atmospheric mercury
534 at Waliguan GAW station, Northwestern China, *Atmospheric Chemistry and Physics*, 12, 1951-1964, 2012a.

535 Fu, X., Feng, X., Shang, L., Wang, S., and Zhang, H.: Two years of measurements of atmospheric total gaseous
536 mercury (TGM) at a remote site in Mt. Changbai area, Northeastern China, *Atmospheric Chemistry and Physics*, 12, 4215-
537 4226, 2012b.

538 Fu, X., Feng, X., Sommar, J., and Wang, S.: A review of studies on atmospheric mercury in China, *Science of the Total*
539 *Environment*, 421, 73-81, 2012c.

540 Fu, X., Maruszczak, N., Heimbürger, L.-E., Sauvage, B., Gheusi, F., Prestbo, E. M., and Sonke, J. E.: Atmospheric
541 mercury speciation dynamics at the high-altitude Pic du Midi Observatory, southern France, *Atmos. Chem. Phys.*, 16, 5623-
542 5639, 2016a.

543 Fu, X., Zhang, H., Yu, B., Wang, X., Lin, C.-J., and Feng, X.: Observations of atmospheric mercury in China: a critical
544 review, *Atmos. Chem. Phys.*, 15, 9455-9476, 2015.

545 Fu, X., Zhu, W., Zhang, H., Sommar, J., Yu, B., Yang, X., Wang, X., Lin, C.-J., and Feng, X.: Depletion of atmospheric
546 gaseous elemental mercury by plant uptake at Mt. Changbai, Northeast China, *Atmospheric Chemistry and Physics*, 16,
547 12861-12873, 2016b.

548 Gautam, R., Hsu, N., Tsay, S., Lau, K., Holben, B., Bell, S., Smirnov, A., Li, C., Hansell, R., and Ji, Q.: Accumulation
549 of aerosols over the Indo-Gangetic plains and southern slopes of the Himalayas: distribution, properties and radiative effects
550 during the 2009 pre-monsoon season, *Atmospheric Chemistry and Physics*, 11, 12841-12863, 2011.

551 Giglio, L., Descloitres, J., Justice, C. O., and Kaufman, Y. J.: An enhanced contextual fire detection algorithm for
552 MODIS, *Remote sensing of environment*, 87, 273-282, 2003.

553 Goodsite, M. E., Plane, J., and Skov, H.: A theoretical study of the oxidation of Hg^0 to $HgBr_2$ in the troposphere,
554 *Environmental science & technology*, 38, 1772-1776, 2004.

555 Gratz, L., Esposito, G., Dalla Torre, S., Cofone, F., Pirrone, N., and Sprovieri, F.: First Measurements of Ambient Total
556 Gaseous Mercury (TGM) at the EvK2CNR Pyramid Observatory in Nepal, *E3S Web of Conferences*, 2013.

557 Holmes, C. D., Jacob, D. J., Corbitt, E. S., Mao, J., Yang, X., Talbot, R., and Slemr, F.: Global atmospheric model for
558 mercury including oxidation by bromine atoms, *Atmospheric Chemistry and Physics*, 10, 12037-12057, 2010.

559 Horowitz, H. M., Jacob, D. J., Zhang, Y., Dibble, T. S., Slemr, F., Amos, H. M., Schmidt, J. A., Corbitt, E. S., Marais,
560 E. A., and Sunderland, E. M.: A new mechanism for atmospheric mercury redox chemistry: implications for the global
561 mercury budget, *Atmospheric Chemistry and Physics*, 17, 6353-6371, 2017.

562 Howard, D., and Edwards, G. C.: Mercury fluxes over an Australian alpine grassland and observation of nocturnal
563 atmospheric mercury depletion events, *Atmos. Chem. Phys. Discuss.*, <https://doi.org/10.5194/acp-2017-580>, in review,
564 2017.

565 Huang, J., Kang, S., Zhang, Q., Yan, H., Guo, J., Jenkins, M. G., Zhang, G., and Wang, K.: Wet deposition of mercury
566 at a remote site in the Tibetan Plateau: concentrations, speciation, and fluxes, *Atmospheric Environment*, 62, 540-550, 2012.

567 Huang, J., Kang, S., Wang, S., Wang, L., Zhang, Q., Guo, J., Wang, K., Zhang, G., and Tripathee, L.: Wet deposition of
568 mercury at Lhasa, the capital city of Tibet, *Science of the total environment*, 447, 123-132, 2013.

569 Huang, J., Kang, S., Guo, J., Zhang, Q., Cong, Z., Sillanpää, M., Zhang, G., Sun, S., and Tripathee, L.: Atmospheric
570 particulate mercury in Lhasa city, Tibetan Plateau, *Atmospheric Environment*, 142, 433-441, 2016.

571 Kang, S., Huang, J., Wang, F., Zhang, Q., Zhang, Y., Li, C., Wang, L., Chen, P., Sharma, C. M., and Li, Q.:
572 Atmospheric mercury depositional chronology reconstructed from lake sediments and ice core in the Himalayas and Tibetan
573 Plateau, *Environmental science & technology*, 50, 2859-2869, 2016.

574 Karunasagar, D., Krishna, M. B., Anjaneyulu, Y. a., and Arunachalam, J.: Studies of mercury pollution in a lake due to
575 a thermometer factory situated in a tourist resort: Kodaikkanal, India, *Environmental pollution*, 143, 153-158, 2006.

576 Kellerhals, M., Beauchamp, S., Belzer, W., Blanchard, P., Froude, F., Harvey, B., McDonald, K., Pilote, M., Poissant,

577 L., and Puckett, K.: Temporal and spatial variability of total gaseous mercury in Canada: results from the Canadian
578 Atmospheric Mercury Measurement Network (CAMNet), *Atmospheric Environment*, 37, 1003-1011, 2003.

579 Kim, S. Y.: Continental outflow of polluted air from the US to the North Atlantic and mercury chemical cycling in
580 various atmospheric environments, University of New Hampshire (Natural Resources and Earth Systems Science Program),
581 2010.

582 Kock, H., Bieber, E., Ebinghaus, R., Spain, T., and Thees, B.: Comparison of long-term trends and seasonal variations
583 of atmospheric mercury concentrations at the two European coastal monitoring stations Mace Head, Ireland, and Zingst,
584 Germany, *Atmospheric Environment*, 39, 7549-7556, 2005.

585 Kocman, D., and Horvat, M.: A laboratory based experimental study of mercury emission from contaminated soils in
586 the River Idrijca catchment, *Atmospheric Chemistry and Physics*, 10, 1417-1426, 2010.

587 Lan, X., Talbot, R., Castro, M., Perry, K., and Luke, W.: Seasonal and diurnal variations of atmospheric mercury across
588 the US determined from AMNet monitoring data, *Atmospheric Chemistry and Physics*, 12, 10569, 2012.

589 Landis, M. S., Stevens, R. K., Schaedlich, F., and Prestbo, E. M.: Development and characterization of an annular
590 denuder methodology for the measurement of divalent inorganic reactive gaseous mercury in ambient air, *Environmental
591 science & technology*, 36, 3000-3009, 2002.

592 Larsen, L., Thomas, C., Eppinga, M., and Coulthard, T.: Exploratory modeling: Extracting causality from complexity,
593 *Eos, Transactions American Geophysical Union*, 95, 285-286, 2014.

594 Li, C., Kang, S., Zhang, Q., and Kaspari, S.: Major ionic composition of precipitation in the Nam Co region, Central
595 Tibetan Plateau, *Atmospheric Research*, 85, 351-360, 2007.

596 Li, C., Bosch, C., Kang, S., Andersson, A., Chen, P., Zhang, Q., Cong, Z., Chen, B., Qin, D., and Gustafsson, Ö.:
597 Sources of black carbon to the Himalayan–Tibetan Plateau glaciers, *Nature Communications*, 7, 12574, 2016.

598 Li, Z., Xia, C., Wang, X., Xiang, Y., and Xie, Z.: Total gaseous mercury in Pearl River Delta region, China during 2008
599 winter period, *Atmospheric Environment*, 45, 834-838, 2011.

600 Lin, C.-J., and Pehkonen, S. O.: The chemistry of atmospheric mercury: a review, *Atmospheric Environment*, 33, 2067-
601 2079, 1999.

602 Lindberg, S. a., and Stratton, W.: Atmospheric mercury speciation: concentrations and behavior of reactive gaseous
603 mercury in ambient air, *Environmental Science & Technology*, 32, 49-57, 1998.

604 Liu, M., Chen, L., Xie, D., Sun, J., He, Q., Cai, L., Gao, Z., and Zhang, Y.: Monsoon-driven transport of atmospheric
605 mercury to the South China Sea from the Chinese mainland and Southeast Asia—Observation of gaseous elemental mercury
606 at a background station in South China, *Environmental Science and Pollution Research*, 23, 21631-21640, 2016.

607 Liu, N., Qiu, G., Landis, M. S., Feng, X., Fu, X., and Shang, L.: Atmospheric mercury species measured in Guiyang,
608 Guizhou province, southwest China, *Atmospheric Research*, 100, 93-102, 2011.

609 Liu, Y., Wang, Y., Pan, Y., and Piao, S.: Wet deposition of atmospheric inorganic nitrogen at five remote sites in the
610 Tibetan Plateau, *Atmospheric Chemistry and Physics*, 15, 11683-11700, 2015.

611 Ma, Y., Kang, S., Zhu, L., Xu, B., Tian, L., and Yao, T.: ROOF OF THE WORLD: Tibetan observation and research
612 platform: atmosphere–land interaction over a heterogeneous landscape, *Bulletin of the American Meteorological Society*, 89,
613 1487-1492, 2008.

614 Mallik, C., and Lal, S.: Seasonal characteristics of SO₂, NO₂, and CO emissions in and around the Indo-Gangetic Plain,
615 Environmental monitoring and assessment, 186, 1295-1310, 2014.

616 Mukherjee, A. B., Bhattacharya, P., Sarkar, A., and Zevenhoven, R.: Mercury emissions from industrial sources in India
617 and its effects in the environment, in: Mercury Fate and Transport in the Global Atmosphere, Springer, 81-112, 2009.

618 Müller, D., Wip, D., Warneke, T., Holmes, C., Dastoor, A., and Notholt, J.: Sources of atmospheric mercury in the
619 tropics: continuous observations at a coastal site in Suriname, Atmospheric Chemistry and Physics, 12, 7391-7397, 2012.

620 Obrist, D., Tas, E., Peleg, M., Matveev, V., Faïn, X., Asaf, D., and Luria, M.: Bromine-induced oxidation of mercury in
621 the mid-latitude atmosphere, Nature Geoscience, 4, 22-26, 2011.

622 Pacyna, E. G., Pacyna, J., Sundseth, K., Munthe, J., Kindbom, K., Wilson, S., Steenhuisen, F., and Maxson, P.: Global
623 emission of mercury to the atmosphere from anthropogenic sources in 2005 and projections to 2020, Atmospheric
624 Environment, 44, 2487-2499, 2010.

625 Park, S.-Y., Holsen, T. M., Kim, P.-R., and Han, Y.-J.: Laboratory investigation of factors affecting mercury emissions
626 from soils, Environmental earth sciences, 72, 2711-2721, 2014.

627 Parvathi, K., Jayaprakash, K., and Sivakumar, N.: Mercury contamination due to thermometer glass solid waste
628 dumping-a preliminary report, Asian Journal of Experimental Chemistry, 5, 46-48, 2010.

629 Peng, G., Qinghua, Y., and Qiufang, W.: Lake ice change at the Nam Co Lake on the Tibetan Plateau during 2000-2013
630 and influencing factors, Progress In Geography, 34, 1241-1249.

631 Peterson, C., Gustin, M., and Lyman, S.: Atmospheric mercury concentrations and speciation measured from 2004 to
632 2007 in Reno, Nevada, USA, Atmospheric Environment, 43, 4646-4654, 2009.

633 Pirrone, N., Cinnirella, S., Feng, X., Finkelman, R., Friedli, H., Leaner, J., Mason, R., Mukherjee, A., Stracher, G., and
634 Streets, D.: Global mercury emissions to the atmosphere from anthropogenic and natural sources, Atmospheric Chemistry
635 and Physics, 10, 5951-5964, 2010.

636 Poissant, L., Pilote, M., Beauvais, C., Constant, P., and Zhang, H. H.: A year of continuous measurements of three
637 atmospheric mercury species (GEM, RGM and Hg p) in southern Quebec, Canada, Atmospheric Environment, 39, 1275-
638 1287, 2005.

639 Polissar, A., Hopke, P., Paatero, P., Kaufmann, Y., Hall, D., Bodhaine, B., Dutton, E., and Harris, J.: The aerosol at
640 Barrow, Alaska: long-term trends and source locations, Atmospheric Environment, 33, 2441-2458, 1999.

641 Rao, S., Zurbenko, I., Neagu, R., Porter, P., Ku, J., and Henry, R.: Space and time scales in ambient ozone data,
642 Bulletin of the American Meteorological Society, 78, 2153-2166, 1997.

643 Schroeder, W. H., and Munthe, J.: Atmospheric mercury—an overview, Atmospheric Environment, 32, 809-822, 1998.

644 Selin, H.: Global environmental law and treaty-making on hazardous substances: the Minamata Convention and
645 mercury abatement, Global Environmental Politics, 14, 1-19, 2014.

646 Sheng, J., Wang, X., Gong, P., Joswiak, D. R., Tian, L., Yao, T., and Jones, K. C.: Monsoon-driven transport of
647 organochlorine pesticides and polychlorinated biphenyls to the Tibetan Plateau: three year atmospheric monitoring study,
648 Environmental science & technology, 47, 3199-3208, 2013.

649 Shia, R. L., Seigneur, C., Pai, P., Ko, M., and Sze, N. D.: Global simulation of atmospheric mercury concentrations and
650 deposition fluxes, Journal of Geophysical Research: Atmospheres, 104, 23747-23760, 1999.

651 Shichang, K., Yongping, Y., and Liping, Z.: Modern Environmental Process and Changes in the Basin of Nam Co in
652 Tibetan Plateau, in, Beijing: China Meteorological Press (in Chinese with English abstract), 2011.

653 Sigler, J., Mao, H., and Talbot, R.: Gaseous elemental and reactive mercury in Southern New Hampshire, *Atmospheric*
654 *Chemistry and Physics*, 9, 1929-1942, 2009.

655 Slemr, F., Brunke, E.-G., Ebinghaus, R., and Kuss, J.: Worldwide trend of atmospheric mercury since 1995,
656 *Atmospheric Chemistry and Physics*, 11, 4779-4787, 2011.

657 Slemr, F., Brunke, E. G., Labuschagne, C., and Ebinghaus, R.: Total gaseous mercury concentrations at the Cape Point
658 GAW station and their seasonality, *Geophysical Research Letters*, 35, 2008.

659 Sprovieri, F., Pirrone, N., Bencardino, M., D'Amore, F., Carbone, F., Cinnirella, S., Mannarino, V., Landis, M.,
660 Ebinghaus, R., and Weigelt, A.: Atmospheric mercury concentrations observed at ground-based monitoring sites globally
661 distributed in the framework of the GMOS network, *Atmospheric Chemistry and Physics*, 16, 11915-11935, 2016.

662 Streets, D. G., Hao, J., Wu, Y., Jiang, J., Chan, M., Tian, H., and Feng, X.: Anthropogenic mercury emissions in China,
663 *Atmospheric Environment*, 39, 7789-7806, 2005.

664 Su, J., Cheng, J.-p., Ye, X., Yuan, T., Wang, W., and Mi, L.: Preliminary study on mercury distribution in multimedia
665 environment in Lanzhou, *Journal of Agro-Environment Science*, 26, 381-385, 2007.

666 Subramanian, V.: Water quality in south Asia, *Asian journal of water, Environment and Pollution*, 1, 41-54, 2004.

667 Sun, X., Wang, K., Kang, S., Guo, J., Zhang, G., Huang, J., Cong, Z., Sun, S., and Zhang, Q.: The role of melting alpine
668 glaciers in mercury export and transport: An intensive sampling campaign in the Qugaqie Basin, inland Tibetan Plateau,
669 *Environmental pollution*, 220, 936-945, 2017.

670 Sun, X., Zhang, Q., Kang, S., Guo, J., Li, X., Yu, Z., Zhang, G., Qu, D., Huang, J., and Cong, Z.: Mercury speciation
671 and distribution in a glacierized mountain environment and their relevance to environmental risks in the inland Tibetan
672 Plateau, *Science of The Total Environment*, 631, 270-278, 2018.

673 Tong, Y., Yin, X., Lin, H., Wang, H., Deng, C., Chen, L., Li, J., Zhang, W., Schauer, J. J., and Kang, S.: Recent
674 Decline of Atmospheric Mercury Recorded by *Androsace tapete* on the Tibetan Plateau, *Environmental Science &*
675 *Technology*, 50, 13224-13231, 2016.

676 Wan, Q., Feng, X., Lu, J., Zheng, W., Song, X., Han, S., and Xu, H.: Atmospheric mercury in Changbai Mountain area,
677 northeastern China I. The seasonal distribution pattern of total gaseous mercury and its potential sources, *Environmental*
678 *research*, 109, 201-206, 2009.

679 Wan, X., Kang, S., Wang, Y., Xin, J., Liu, B., Guo, Y., Wen, T., Zhang, G., and Cong, Z.: Size distribution of
680 carbonaceous aerosols at a high-altitude site on the central Tibetan Plateau (Nam Co Station, 4730 m asl), *Atmospheric*
681 *Research*, 153, 155-164, 2015.

682 Wang, B., and Fan, Z.: Choice of South Asian summer monsoon indices, *Bulletin of the American Meteorological*
683 *Society*, 80, 629-638, 1999.

684 Wang, B., Wu, R., and Lau, K.: Interannual variability of the Asian summer monsoon: Contrasts between the Indian
685 and the western North Pacific–East Asian monsoons, *Journal of climate*, 14, 4073-4090, 2001.

686 Wang, Y., Zhang, X., and Draxler, R. R.: TrajStat: GIS-based software that uses various trajectory statistical analysis
687 methods to identify potential sources from long-term air pollution measurement data, *Environmental Modelling & Software*,

688 24, 938-939, 2009.

689 Wang, Y.: *MeteoInfo: GIS software for meteorological data visualization and analysis*, *Meteorological Applications*,
690 21, 360-368, 2014.

691 Wang, Y., Zhang, Y., Schauer, J. J., de Foy, B., Guo, B., and Zhang, Y.: Relative impact of emissions controls and
692 meteorology on air pollution mitigation associated with the Asia-Pacific Economic Cooperation (APEC) conference in
693 Beijing, China, *Science of The Total Environment*, 571, 1467-1476, 2016.

694 Wang, Y., de Foy, B., Schauer, J. J., Olson, M. R., Zhang, Y., Li, Z., and Zhang, Y.: Impacts of regional transport on
695 black carbon in Huairou, Beijing, China, *Environmental Pollution*, 221, 75-84, 2017.

696 Weiss-Penzias, P., Jaffé, D. A., McClintick, A., Prestbo, E. M., and Landis, M. S.: Gaseous elemental mercury in the
697 marine boundary layer: Evidence for rapid removal in anthropogenic pollution, *Environmental science & technology*, 37,
698 3755-3763, 2003.

699 Wu, Q., Wang, S., Li, G., Liang, S., Lin, C.-J., Wang, Y., Cai, S., Liu, K., and Hao, J.: Temporal Trend and Spatial
700 Distribution of Speciated Atmospheric Mercury Emissions in China During 1978–2014, *Environmental Science &
701 Technology*, 50, 13428-13435, 2016.

702 Wu, Q., Gao, W., Wang, S., and Hao, J.: Updated atmospheric speciated mercury emissions from iron and steel
703 production in China during 2000–2015, *Atmospheric Chemistry and Physics*, 17, 10423-10433, 2017.

704 Xia, X., Zong, X., Cong, Z., Chen, H., Kang, S., and Wang, P.: Baseline continental aerosol over the central Tibetan
705 plateau and a case study of aerosol transport from South Asia, *Atmospheric environment*, 45, 7370-7378, 2011.

706 Xiao, H., Shen, L., Su, Y., Barresi, E., DeJong, M., Hung, H., Lei, Y.-D., Wania, F., Reiner, E. J., and Sverko, E.:
707 Atmospheric concentrations of halogenated flame retardants at two remote locations: The Canadian High Arctic and the
708 Tibetan Plateau, *Environmental pollution*, 161, 154-161, 2012.

709 Xiu, G., Cai, J., Zhang, W., Zhang, D., Büeler, A., Lee, S., Shen, Y., Xu, L., Huang, X., and Zhang, P.: Speciated
710 mercury in size-fractionated particles in Shanghai ambient air, *Atmospheric Environment*, 43, 3145-3154, 2009.

711 Xu, L., Chen, J., Yang, L., Niu, Z., Tong, L., Yin, L., and Chen, Y.: Characteristics and sources of atmospheric mercury
712 speciation in a coastal city, Xiamen, China, *Chemosphere*, 119, 530-539, 2015.

713 Yang, H., Battarbee, R. W., Turner, S. D., Rose, N. L., Derwent, R. G., Wu, G., and Yang, R.: Historical reconstruction
714 of mercury pollution across the Tibetan Plateau using lake sediments, *Environmental science & technology*, 44, 2918-2924,
715 2010.

716 Yaqiong, L., Yaoming, M., and Maoshan, L.: Study on characteristic of atmospheric boundary layer over Lake Namco
717 region, Tibetan Plateau, *Plateau Meteorology (in Chinese)*, 27, 1205-1210, 2008.

718 Yatavelli, R. L., Fahrni, J. K., Kim, M., Crist, K. C., Vickers, C. D., Winter, S. E., and Connell, D. P.: Mercury, PM 2.5
719 and gaseous co-pollutants in the Ohio River Valley region: Preliminary results from the Athens supersite, *Atmospheric
720 environment*, 40, 6650-6665, 2006.

721 Yin, X., Kang, S., de Foy, B., Cong, Z., Luo, J., Lang, Z., Ma, Y., Zhang, G., Rupakheti, D., and Zhang, Q.: Surface
722 ozone at Nam Co in the inland Tibetan Plateau: variation, synthesis comparison and regional representativeness,
723 *Atmospheric Chemistry and Physics*, 17, 11293-11311, 2017.

724 You, Q., Kang, S., Li, C., Li, M., and Liu, J.: Variation features of meteorological elements at Namco Station, Tibetan

725 Plateau, *Meteorological Monthly*, 33, 54-60, 2007.

726 Yu, B., Wang, X., Lin, C. J., Fu, X., Zhang, H., Shang, L., and Feng, X.: Characteristics and potential sources of
727 atmospheric mercury at a subtropical near - coastal site in East China, *Journal of Geophysical Research: Atmospheres*, 120,
728 8563-8574, 2015.

729 Zhang, L., Wang, S., Wang, L., and Hao, J.: Atmospheric mercury concentration and chemical speciation at a rural site
730 in Beijing, China: implications of mercury emission sources, *Atmospheric Chemistry and Physics*, 13, 10505-10516, 2013.

731 Zhang, Q., Pan, K., Kang, S., Zhu, A., and Wang, W.-X.: Mercury in wild fish from high-altitude aquatic ecosystems in
732 the Tibetan Plateau, *Environmental science & technology*, 48, 5220-5228, 2014.

733 Zhang, H., Fu, X., Lin, C., Wang, X., and Feng, X.: Observation and analysis of speciated atmospheric mercury in
734 Shangri-La, Tibetan Plateau, China, *Atmos. Chem. Phys.*, 15, 653-665, 2015.

735 Zhang, X., Ming, J., Li, Z., Wang, F., and Zhang, G.: The online measured black carbon aerosol and source orientations
736 in the Nam Co region, Tibet, *Environmental Science and Pollution Research*, 24, 25021-25033, 2017.

737 Zhang, Y., Jacob, D. J., Horowitz, H. M., Chen, L., Amos, H. M., Krabbenhoft, D. P., Slemr, F., Louis, V. L. S., and
738 Sunderland, E. M.: Observed decrease in atmospheric mercury explained by global decline in anthropogenic emissions,
739 *Proceedings of the National Academy of Sciences*, 113, 526-531, 2016.

740 Zhu, J., Wang, T., Talbot, R., Mao, H., Hall, C., Yang, X., Fu, C., Zhuang, B., Li, S., and Han, Y.: Characteristics of
741 atmospheric total gaseous mercury (TGM) observed in urban Nanjing, China, *Atmospheric Chemistry and Physics*, 12,
742 12103-12118, 2012.

743

744

745

746

747

748

749

750

751

752

753

754

755

756

757

758

759

760

761

762

763

764

Table 1. The statistics of TGM and meteorological variables in different seasons at the Nam Co Station during the measurement period (2012-2014).

Period	Statistical	TGM (ng m ⁻³)	T (°C)	RH (%)	WS (m s ⁻¹)
Total	Mean	1.33	-0.29	50.67	3.32
	Median	1.34	0.30	50.00	2.80
	Standard Deviation	0.24	8.98	22.37	2.22
	Minimum	0.23	-28.90	5.30	0.00
	Maximum	3.14	19.00	98.00	15.60
	Count	14408	20695	20695	20695
Spring (MAM)	Mean	1.28	-0.90	51.58	3.21
	Median	1.30	-0.60	50.30	2.80
	Standard Deviation	0.20	6.48	24.38	2.11
	Minimum	0.42	-21.20	5.30	0.00
	Maximum	2.41	17.90	98.00	12.80
	Count	4506	4980	4980	4980
Summer (JJA)	Mean	1.50	8.80	63.32	2.94
	Median	1.50	8.60	65.30	2.60
	Standard Deviation	0.20	3.59	18.25	1.74
	Minimum	0.23	-4.10	11.00	0.00
	Maximum	3.14	19.00	97.00	11.10
	Count	5243	5805	5805	5805
Autumn (SON)	Mean	1.22	-0.78	47.06	3.36
	Median	1.20	-0.40	46.00	2.90
	Standard Deviation	0.17	7.23	20.55	2.07
	Minimum	0.87	-24.80	8.00	0.00
	Maximum	2.68	14.60	97.00	12.90
	Count	2267	4800	4800	4800
Winter (DJF)	Mean	1.14	-9.57	38.81	3.83
	Median	1.13	-9.00	36.00	3.00
	Standard Deviation	0.18	6.40	18.36	2.78
	Minimum	0.45	-28.90	7.00	0.00
	Maximum	2.08	5.20	91.70	15.60
	Count	2392	5110	5110	5110

765

766

767

768

769

Table 2. Statistics of free parameters in the box model of TGM at the Nam Co Station by seasons.

	Initial	Morning	Evening TGM	Constant	Free	TGM	root-mean-	R²
	TGM	TGM (7-9)	(18-22) burst	TGM	tropospheric	lifetime during	square error	
	(ng m⁻³)	burst	(ng m⁻²h⁻¹)	deposition	TGM	daylight	(RMSE)	
		(ng m⁻²h⁻¹)		(ng m⁻²h⁻¹)	(ng m⁻³)	(day)		
Spring	1.288	58.29	37.66	-1.658	1.228	3.183	0.00983	0.96
Summer	1.521	14.2	25.65	-1.775	1.553	5.991	0.00796	0.91
Autumn	1.211	53.34	9.144	-1.061	1.036	Inf	0.0086	0.93
Winter	1.115	52.92	2.468	0	1.168	2.984	0.00368	0.99

770

771

772

773

774

775

776

777

778

779

780

781

782

783

784

785

786

787

788

789

790

791

792

793

794

795

796

Table 3. Contribution from the different groups to the total variance of the model. The standard deviation of each group gives a sense of the contribution of each group to the variance in units of ng m⁻³. The variance contribution shows the percentage that each group contributes to the total variance of the model.

Group name	No. Variables	Std (ng m⁻³)	Variance Contribution (%)
Seasonal Signal	6	0.161	83.70
Diurnal Signal	24	0.036	4.08
WRF PBLH	5	0.034	3.81
Surface O ₃ Conc	1	0.032	3.20
Strat. O ₃ Tracer	1	0.031	3.04
Local Winds	20	0.020	1.34
Annual Signal	43	0.016	0.86

797

798

799

800

801

802

803

804

805

806

807

808

809

810

811

812

813

814

815

816

817

818

819

820

821

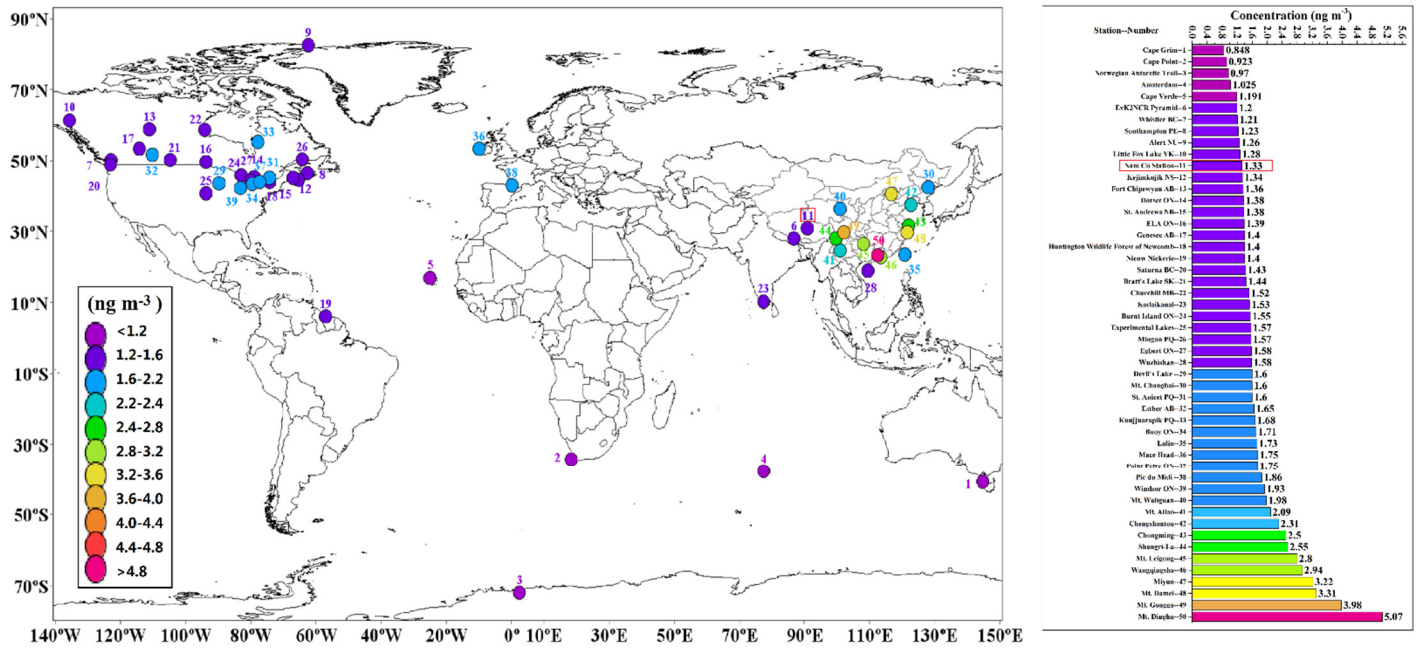
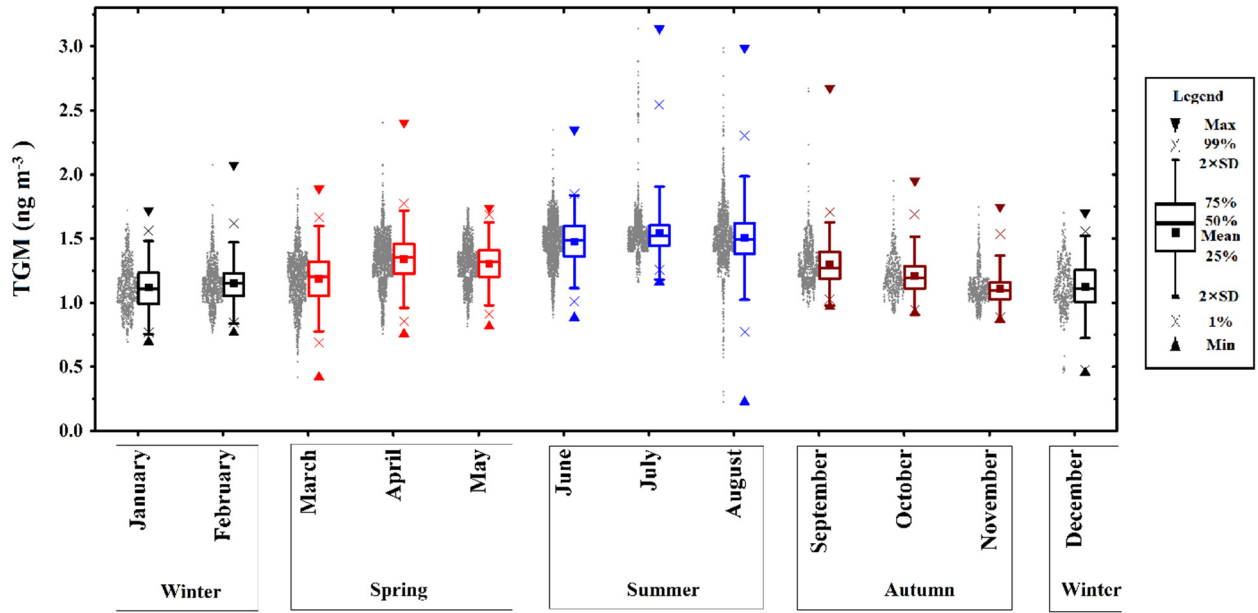


Fig. 1. Geographical location of the remote and rural sites with atmospheric mercury measurements.

823
824
825
826
827
828
829
830
831
832
833
834
835
836
837
838
839
840
841



843

844

Fig. 2. Monthly average and statistical parameters of TGM at the Nam Co Station during the whole measurement period (spring (MAM) in red; summer (JJA) in blue; autumn (SON) in dark red; winter (DJF) in black).

845

846

847

848

849

850

851

852

853

854

855

856

857

858

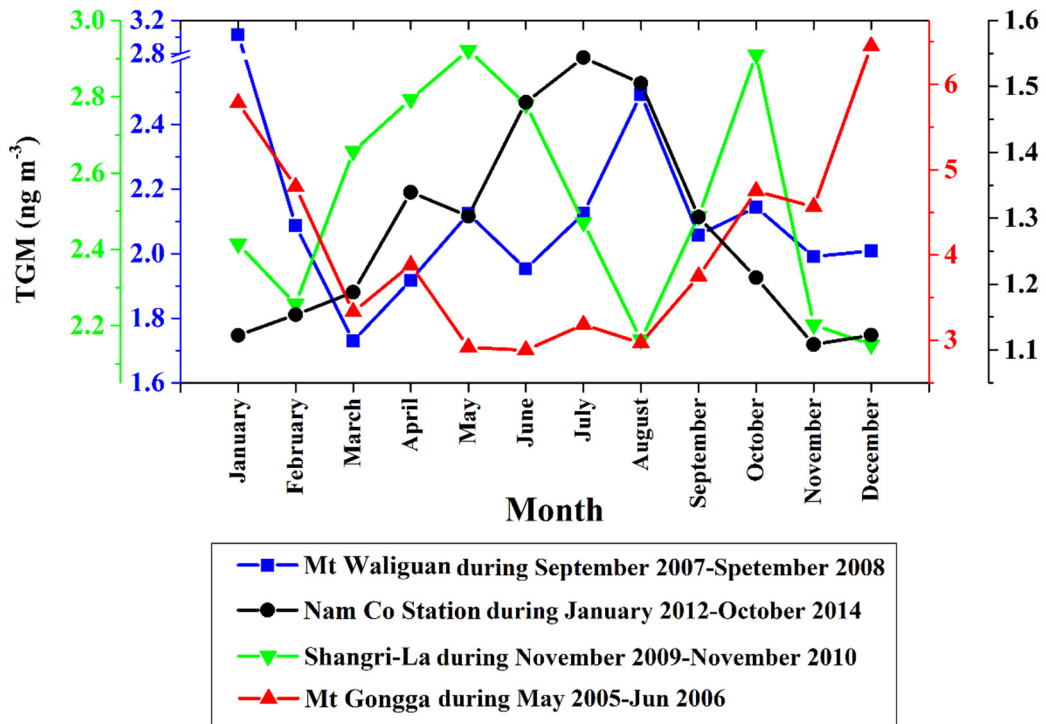
859

860

861

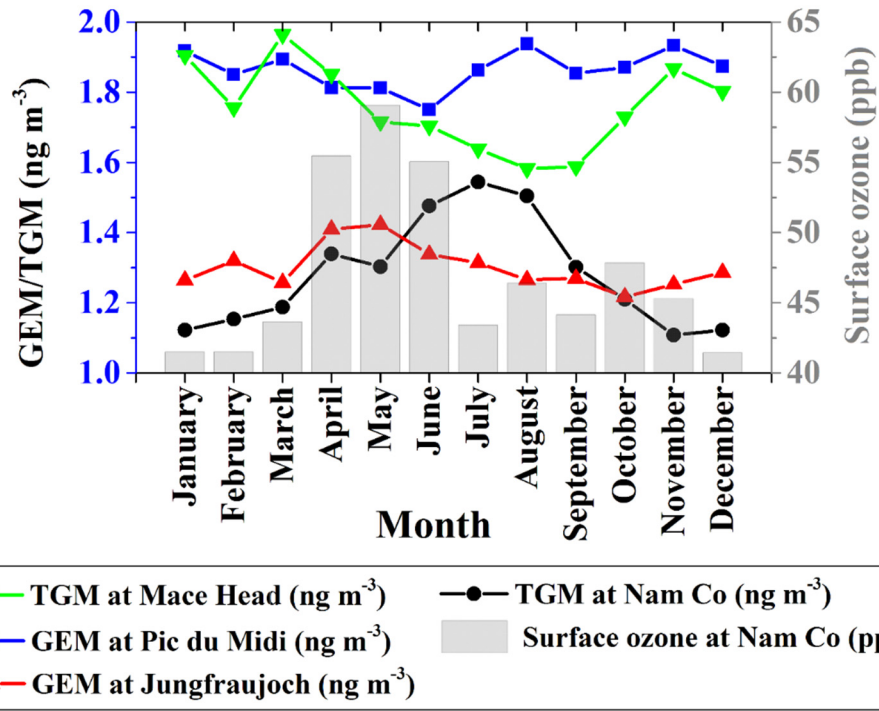
862

863
864

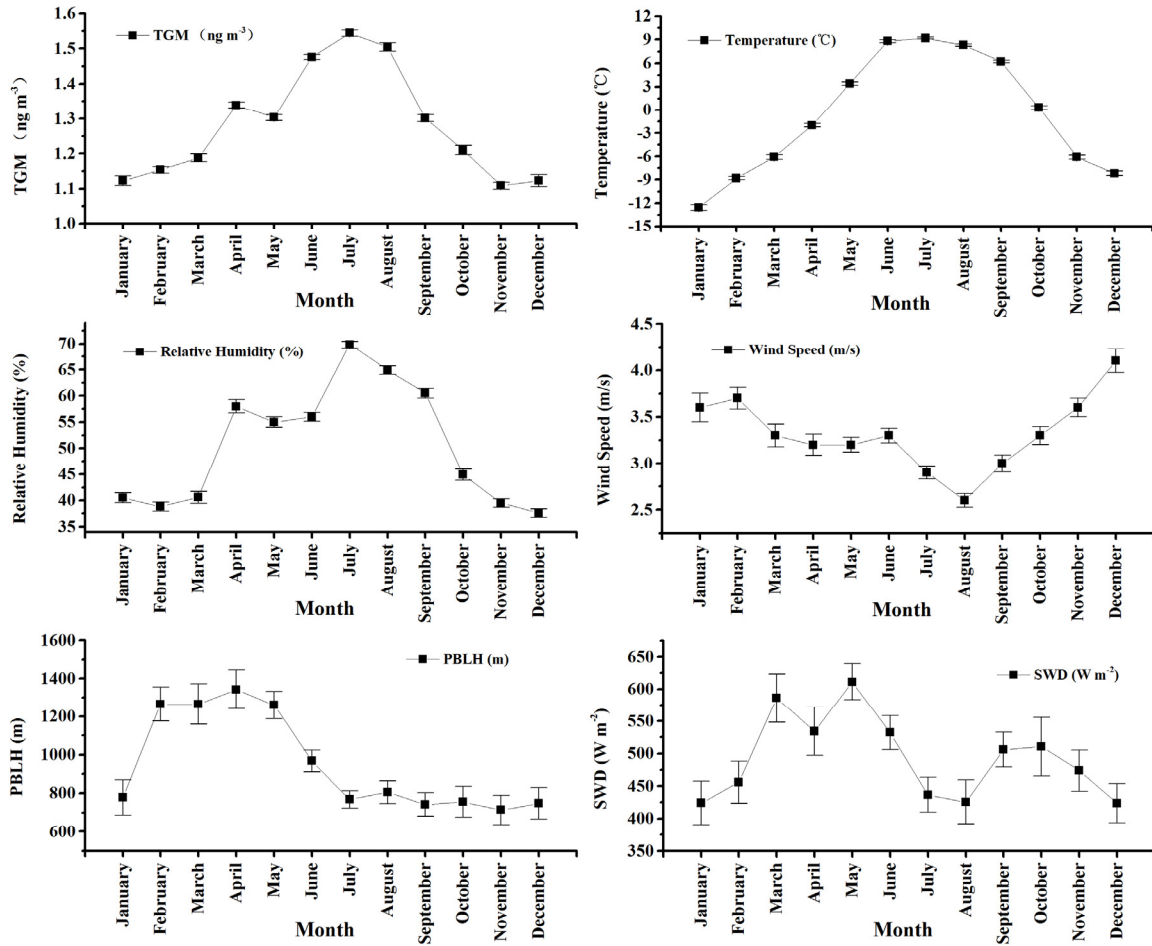


865
866
867
868
869
870
871
872
873
874
875
876
877
878
879
880
881

Fig. 3. Variations of monthly mean TGM at four sites (Mt. Waliguan (Fu et al., 2012a), Nam Co, Mt. Gongga (Fu et al., 2008) and Shangri-La (Zhang et al., 2015)) in the Tibetan Plateau.



883
 884 Fig. 4. Monthly average GEM/TGM at the Nam Co Station and three high-altitude background stations in the Northern
 885 Hemisphere (Denzler et al., 2017; Fu et al., 2016a; Ebinghaus et al., 2002) (average TGM at Mace Head in green; average GEM at
 886 Pic du Midi in blue; median GEM at Jungfrauoch in red; average TGM at the Nam Co Station in black); and monthly average
 887 surface ozone at Nam Co in column.
 888
 889
 890
 891
 892
 893
 894
 895
 896
 897
 898
 899
 900
 901



903
 904
 905
 906
 907
 908
 909
 910
 911
 912
 913
 914
 915
 916

Fig. 5. Monthly variations of TGM, relative humidity, temperature, SWD (downward shortwave radiation), wind speed and PBLH (planetary boundary layer height) during the whole measurement period at the Nam Co Station. Error bars are 95% confidence levels.

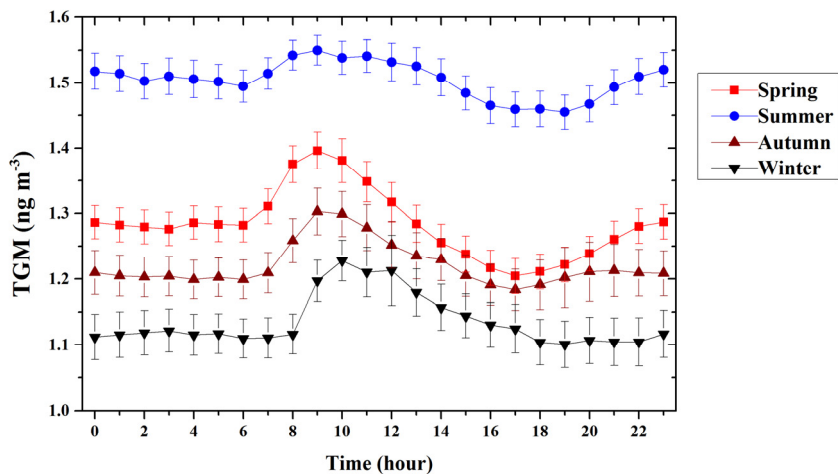
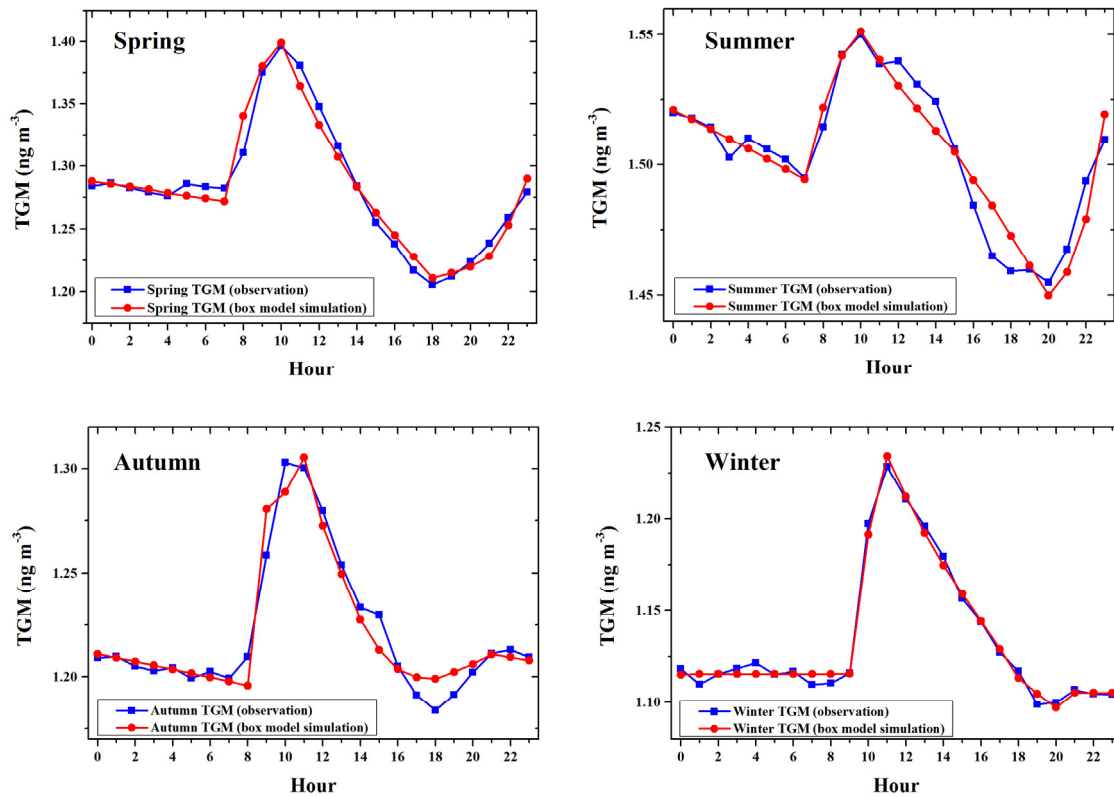


Fig. 6. Diurnal profiles of average hourly TGM at the Nam Co Station by seasons during the measurement period. Error bars are 95% confidence levels.

918
 919
 920
 921
 922
 923
 924
 925
 926
 927
 928
 929
 930
 931
 932
 933
 934
 935
 936
 937
 938
 939



941

942

Fig. 7. Diurnal profiles of average hourly TGM at the Nam Co Station by seasons during the measurement period compared with box model simulation.

943

944

945

946

947

948

949

950

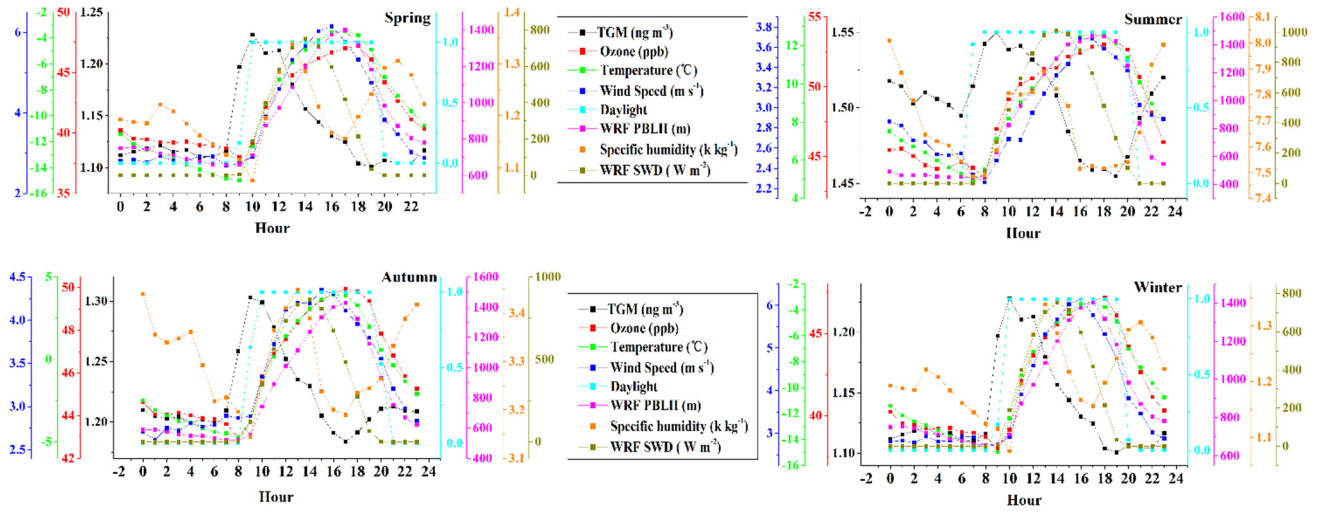
951

952

953

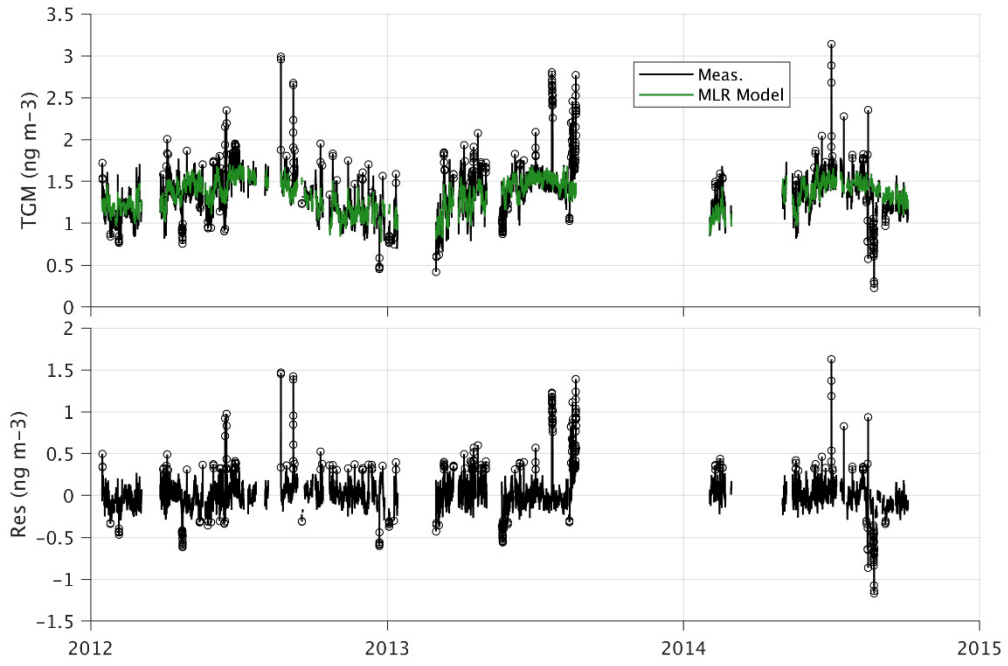
954

955



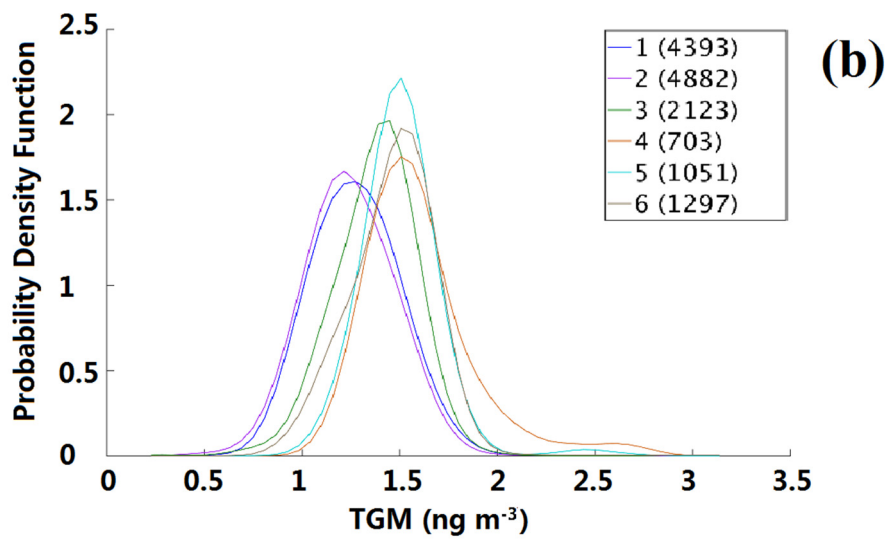
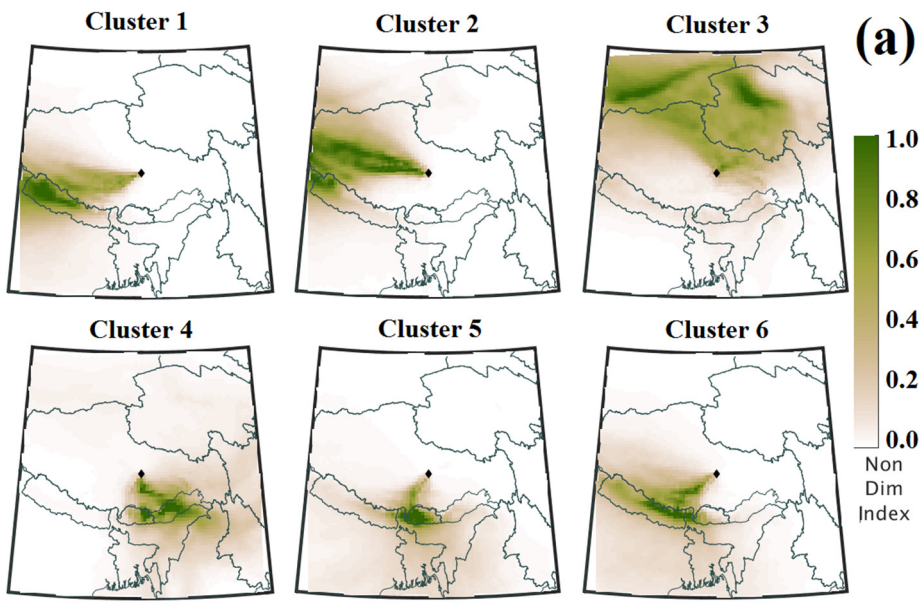
957
 958
 959
 960
 961
 962
 963
 964
 965
 966
 967
 968
 969
 970
 971
 972
 973
 974
 975
 976
 977
 978

Fig. 8. Diurnal profiles of TGM, ozone and meteorological parameters (temperature, wind speed, daylight, WRF PBLH (planetary boundary layer height), specific humidity and WRF SWD (downward shortwave radiation)) at the Nam Co Station by seasons for the measurement period.



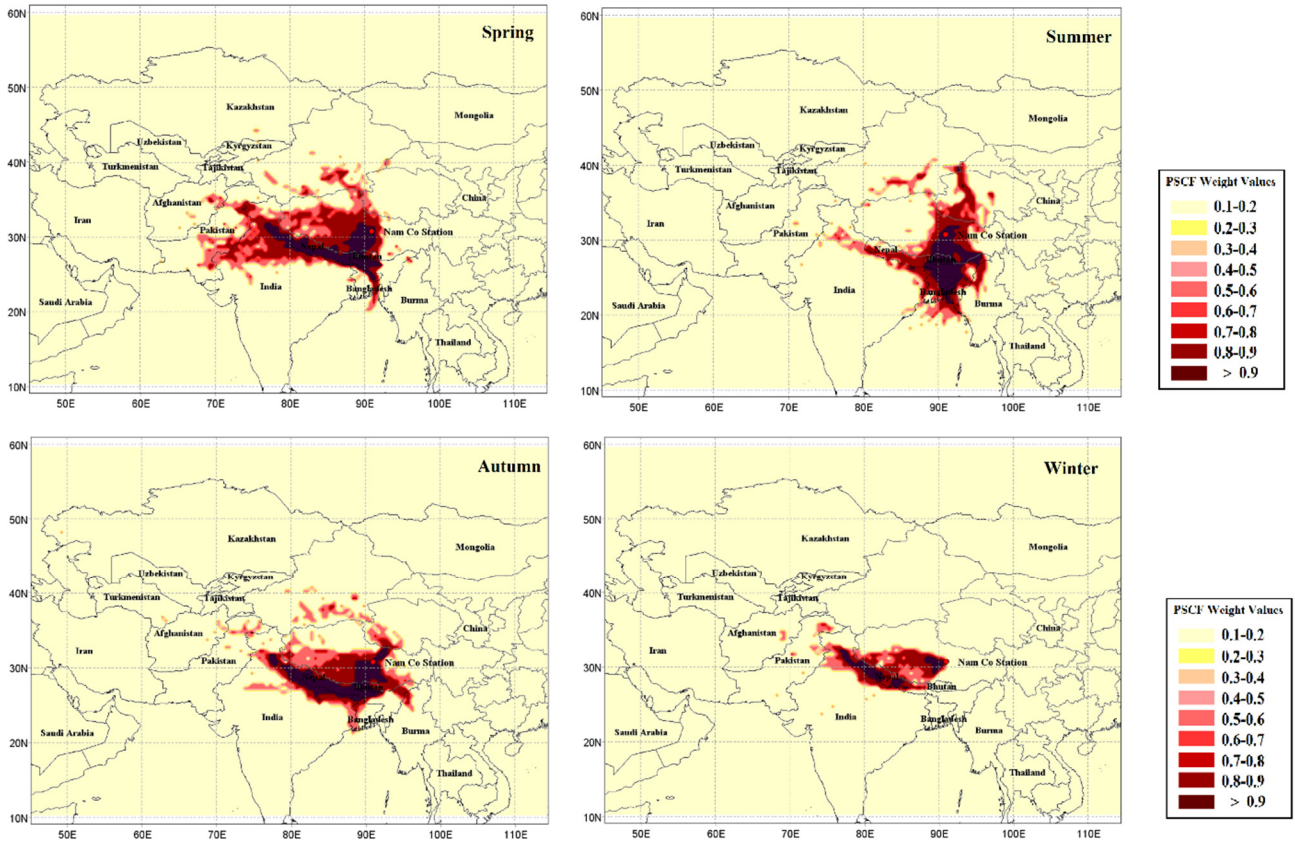
980
981
982
983
984
985
986
987
988
989
990
991
992
993
994
995
996
997
998
999

Fig. 9. The measurements and Multi Linear Regression (MLR) model of TGM (top) and model residual (bottom) (residual = measurement – simulation). The outliers are shown as circles.



1001
1002
1003
1004
1005
1006

Fig. 10. Clusters of air mass transport to Nam Co using WRF-FLEXPART back-trajectories (a) and probability density function of TGM concentrations for each cluster, with number of data points in each cluster in parentheses (b).



1008

1009

Fig. 11. Potential Source Contribution Function showing areas with possible emissions or air mass transport associated with higher TGM concentrations at the Nam Co Station by seasons in 2012.

1010

1011

1012

1013

1014

1015

1016

1017

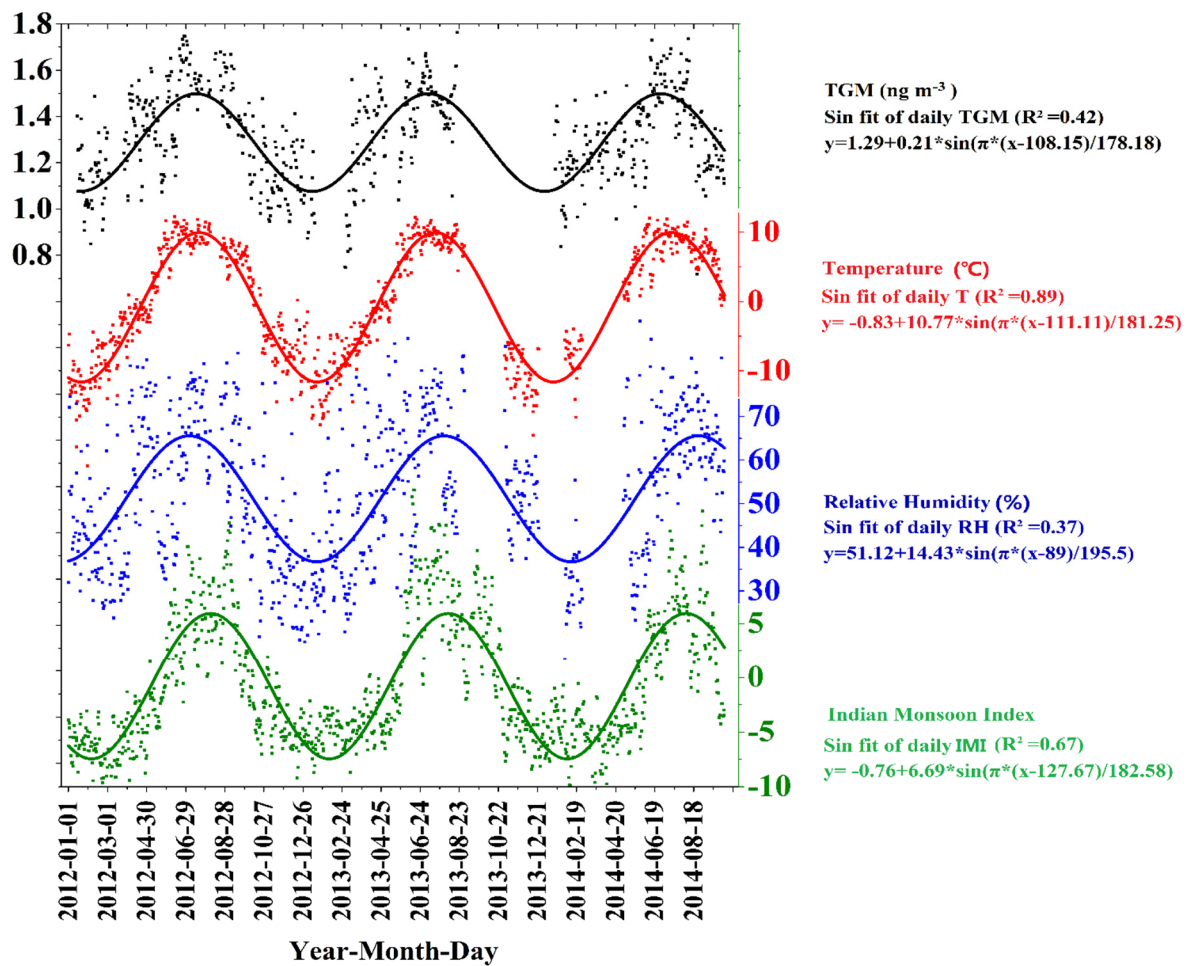
1018

1019

1020

1021

1022



1024

1025

1026 Fig. 12. Series of daily mean TGM, temperature, relative humidity and Indian Monsoon Index and their sinusoidal curve fits.

1027

1028